Electronic Supplementary Material (ESI) for Dalton Transactions.


# Syntheses and characterization of hepta-coordinated Group 4 amidinate complexes

*Tabitha M. Cook,*[1,2] *Carlos A. Steren*[1] *and Zi-Ling Xue*[1,*]

[1] Department of Chemistry, University of Tennessee, Knoxville, Tennessee 37996, USA

[2] Department of Chemistry and Biochemistry, Berry College, Mount Berry, Georgia 30149, USA

## *Supplementary Information*

## Table of Contents

**Fig. S1**..... S-4

**Fig. S2**..... S-5

**Table S1**.....S-6

**Table S2**.....S-8

**Tables S3** and **S4**.....S-10

**Table S5**.....S-11

**Table S6**.....S-12

**Figs. S3** and **S4**.....S-13

**Figs. S5** and **S6**.....S-14

**Figs. S7** and **S8**.....S-15

**Figs. S9** and **S10**.....S-16

**Figs. S11** and **S12**.....S-17

**Figs. S13** and **S14**.....S-18

**Figs. S15** and **S16**.....S-19

**Figs. S17** and **S18**.....S-20

**Figs. S19** and **S20**.....S-21

**Figs. S21** and **S22**.....S-22

**Figs. S23** and **S24**.....S-23

**Figs. S25** and **S26**.....S-24

**Figs. S27** and **S28**.....S-25

**Figs. S29** and **S30**.....S-26

**Figs. S31** and **S32**.....S-27

**Figs. S33** and **S34**……S-28

**Fig. S35**……S-29

**Fig. S36**……S-30

**Table S7**……S-31

**Figs. S37** and **S38**……S-32

**Figs. S39** and **S40**……S-33

**Fig. S41**……S-34

**Table S8**……S-35

**Figs. S42** and **S43**……S-36

**Fig. S44**……S-37

**Figs. S45** and **S46**……S-38

**Figs. S47** and **S48**……S-39

**Figs. S49** and **S50**……S-40

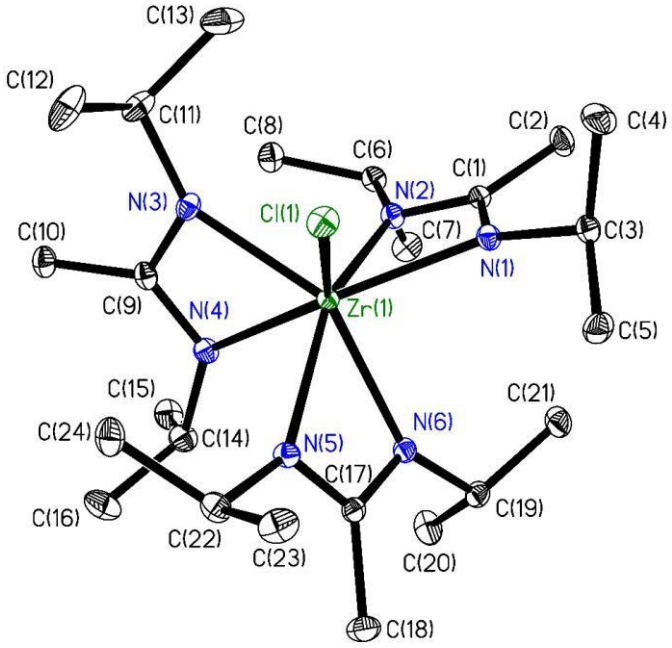


**Fig. S1.** ORTEP of Zr-Cl (**1**) at 100(2) K. Thermal ellipsoids are 30% probability level. H atoms were removed for clarity.

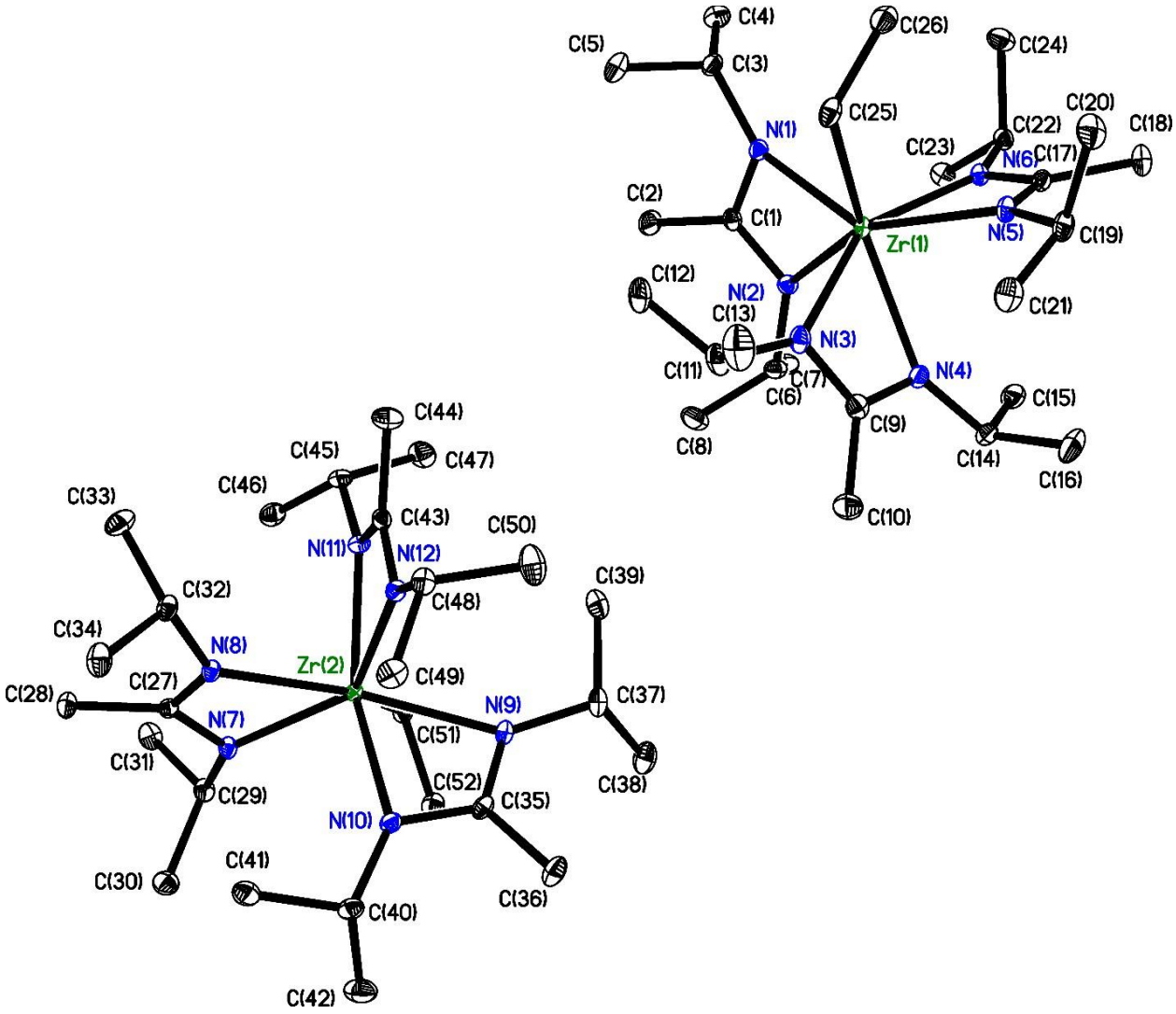


**Fig. S2.** ORTEP of Zr-Et (**5**) at 100(2) K showing two slightly different molecules of Zr-Et (**5**). Thermal ellipsoids are 30% probability level. H atoms were removed for clarity.

**Table S1.** Crystal data and structure refinement for Zr-Cl (**1**) and Hf-Cl (**2**)

| Complex | Zr-Cl (**1**) | Hf-Cl (**2**) |
|---|---|---|
| Empirical formula | $C_{24}H_{51}N_6ClZr$ | $C_{24}H_{51}N_6ClHf$ |
| Formula weight | 550.37 | 637.64 |
| Temperature | 100(2) K | 100(2) K |
| Wavelength | 0.71073 Å | 0.71073 Å |
| Crystal System | Monoclinic | Monoclinic |
| Space Group | $P2_1/n$ | $P2_1/n$ |
| Unit cell dimensions | $a$ = 10.447(2) Å<br>$\alpha$ = 90° | $a$ = 10.4324(15) Å<br>$\alpha$ = 90° |
| | $b$ = 16.453(3) Å<br>$\beta$ = 93.334° | $b$ = 16.447(2) Å<br>$\beta$ = 93.053(2)° |
| | $c$ = 17.100(3) Å<br>$\gamma$ = 90° | $c$ = 17.091(2) Å<br>$\gamma$ = 90° |
| Volume | 2934.5(8) Å$^3$ | 2928.3(7) Å$^3$ |
| $Z$ | 4 | 4 |
| Density (calculated) | 1.246 g/cm$^3$ | 1.446 g/cm$^3$ |
| Absorption coefficient | 0.487 mm$^{-1}$ | 3.675 mm$^{-1}$ |
| $F$(000) | 1176 | 1304.0 |
| Crystal size | 0.358 x 0.219 x 0.203 mm$^3$ | 0.271 × 0.251 × 0.233 mm$^3$ |
| Theta range for data collection | 2.23 to 27.91° | 2.24 to 27.94° |
| Index ranges | -13 ≤ $h$ ≤ 13, 0 ≤ $k$ ≤ 21, 0 ≤ $l$ ≤ 22 | -13 ≤ $h$ ≤ 13, 0 ≤ $k$ ≤ 21, 0 ≤ $l$ ≤ 22 |
| Reflections collected | 6921 | 6975 |
| Independent reflections | 6921 [$R_{int}$ = 0.000] | 6975 [$R_{int}$ = 0.000] |
| Completeness | 98.4% | 93.0% |
| Max. and min. transmission | 0.746 and 0.658 | 0.745 and 0.491 |

| | | |
|---|---|---|
| Refinement method | Full-matrix least-squares on $F^2$ | Full-matrix least-squares on $F^2$ |
| Absorption correction | Semi-empirical from equivalents | Semi-empirical from equivalents |
| Data / restraints / parameters | 6921 / 0 / 305 | 6975 / 0 / 305 |
| Goodness-of-fit on $F^2$ | 1.031 | 1.186 |
| Final $R$ indices [$I > 2\sigma(I)$] | $R1$ = 0.0269, w$R2$ = 0.0639 | $R1$ = 0.0445, w$R2$ = 0.1177 |
| $R$ indices (all data) | $R1$ = 0.0307, w$R2$ = 0.0662 | $R1$ = 0.0525, w$R2$ = 0.1213 |
| Largest diff. peak and hole | 0.51 and -0.40 eÅ$^{-3}$ | 5.33 and -2.24 eÅ$^{-3}$ |

[a] $R1 = \Sigma||F_o| - |F_c|| / \Sigma|F_o|$; $wR2 = [\Sigma\, w(F_o^2 - F_c^2)^2 / \Sigma\, w(F_o^2)^2]^{1/2}$;

$w = 1/[\sigma^2(F_o) + (aP)^2 + bP]$; $P = [2Fc^2 + \mathrm{Max}(F_o^2, 0)]/3$

**Table S2.** Crystal data and structure refinement for Zr-Et (**5**) and Hf-Et (**6**)

| Complex | Zr-Et (**5**) | Hf-Et (**6**) |
|---|---|---|
| Empirical formula | $C_{26}H_{56}N_6Zr$ | $C_{26}H_{56}N_6Hf$ |
| Formula weight | 549.98 | 631.25 |
| Temperature | 100(2) K | 100(2) K |
| Wavelength | 0.71073 Å | 0.71073 Å |
| Crystal System | Monoclinic | Monoclinic |
| Space Group | $P2_1/c$ | $P2_1/c$ |
| Unit cell dimensions | $a$ = 21.699(7) Å<br>$\alpha$ = 90°<br>$b$ = 15.619(5) Å<br>$\beta$ = 103.401(4)°<br>$c$ = 18.597(6) Å<br>$\gamma$= 90° | $a$ = 21.658(7) Å<br>$\alpha$ = 90°<br>$b$ = 15.566(5) Å<br>$\beta$ = 103.681(4)°<br>$c$ = 18.594(6) Å<br>$\gamma$ = 90° |
| Volume | 6131(3) Å$^3$ | 6091(3) Å$^3$ |
| $Z$ | 8 | 8 |
| Density (calculated) | 1.179 g/cm$^3$ | 1.377 g/cm$^3$ |
| Absorption coefficient | 0.381 mm$^{-1}$ | 3.448 mm$^{-1}$ |
| $F$(000) | 2352.0 | 2608.0 |
| Crystal size | 0.552 × 0.382 × 0.152 mm$^3$ | 0.404 × 0.381 × 0.32 mm$^3$ |
| Theta range for data collection | 1.62 to 27.74° | 1.67 to 27.83° |
| Index ranges | $-28 \le h \le 28$, $-20 \le k \le 20$, $-24 \le l \le 24$ | $-27 \le h \le 27$, $-20 \le k \le 20$, $-24 \le l \le 24$ |
| Reflections collected | 69813 | 69357 |
| Independent reflections | 14282 [$R_{int}$ = 0.0330] | 14157 [$R_{int}$ = 0.0333] |
| Completeness | 99.0% | 97.8% |
| Max. and min. transmission | 0.746 and 0.658 | 0.746 and 0.485 |
| Refinement method | Full-matrix least-squares on $F^2$ | Full-matrix least-squares on $F^2$ |

| | | |
|---|---|---|
| Absorption correction | Semi-empirical from equivalents | Semi-empirical from equivalents |
| Data / restraints / parameters | 14282 / 0 / 627 | 14162 / 0 / 627 |
| Goodness-of-fit on $F^2$ | 1.046 | 1.040 |
| Final $R$ indices [$I > 2\sigma(I)$] | $R1$ = 0.0273, w$R2$ = 0.0643 | $R1$ = 0.0199, w$R2$ = 0.0467 |
| $R$ indices (all data) | $R1$ = 0.0332, w$R2$ = 0.0679 | $R1$ = 0.0223, w$R2$ = 0.0477 |
| Largest diff. peak and hole | 0.51 and -0.44 eÅ$^{-3}$ | 0.83 and -1.08 eÅ$^{-3}$ |

[a] $R1 = \Sigma||F_o| - |F_c|| / \Sigma|F_o|$; $wR2 = [\Sigma\, w(F_o^2 - F_c^2)^2 / \Sigma\, w(F_o^2)^2]^{1/2}$;

$w = 1/[\sigma^2(F_o) + (aP)^2 + bP]$; $P = [2Fc^2 + \mathrm{Max}(F_o^2, 0)]/3$

**Table S3.** Selected distances and angles for Zr-Cl (**1**)

| **Distances (Å)** | | | |
|---|---|---|---|
| Zr(1)-Cl(1) | 2.5125(5) | Zr(1)-N(4) | 2.2814(13) |
| Zr(1)-N(1) | 2.2141(14) | Zr(1)-N(5) | 2.2172(13) |
| Zr(1)-N(2) | 2.3154(14) | Zr(1)-N(6) | 2.3175(13) |
| Zr(1)-N(3) | 2.2015(14) | | |
| **Angles (°)** | | | |
| N(1)-Zr(1)-Cl(1) | 82.71(4) | N(3)-Zr(1)-N(4) | 58.96(5) |
| N(2)-Zr(1)-Cl(1) | 123.82(4) | N(3)-C(9)-N(4) | 111.82(14) |
| N(1)-Zr(1)-N(2) | 58.64(5) | N(5)-Zr(1)-Cl(1) | 84.72(3) |
| N(1)-C(1)-N(2) | 112.78(14) | N(6)-Zr(1)-Cl(1) | 125.68(4) |
| N(3)-Zr(1)-Cl(1) | 84.96(4) | N(5)-Zr(1)-N(6) | 58.57(5) |
| N(4)-Zr(1)-Cl(1) | 132.45(4) | N(5)-C(17)-N(6) | 112.79(14) |

**Table S4.** Selected distances and angles for Hf-Cl (**2**)

| **Distances (Å)** | | | |
|---|---|---|---|
| Hf(1)-Cl(1) | 2.5014(16) | Hf(1)-N(4) | 2.306(6) |
| Hf(1)-N(1) | 2.183(6) | Hf(1)-N(5) | 2.202(6 |
| Hf(1)-N(2) | 2.259(5) | Hf(1)-N(6) | 2.293(6) |
| Hf(1)-N(3) | 2.199(6) | | |
| **Angles (°)** | | | |
| N(1)-Hf(1)-Cl(1) | 84.30(16) | N(3)-Hf(1)-N(4) | 58.9(2) |
| N(2)-Hf(1)-Cl(1) | 132.08(16) | N(3)-C(9)-N(4) | 112.6(6) |
| N(1)-Hf(1)-N(2) | 59.2(2) | N(5)-Hf(1)-Cl(1) | 82.36(16) |
| N(1)-C(1)-N(2) | 110.3(6) | N(6)-Hf(1)-Cl(1) | 123.58(15) |
| N(3)-Hf(1)-Cl(1) | 84.52(15) | N(5)-Hf(1)-N(6) | 59.2(2) |
| N(4)-Hf(1)-Cl(1) | 125.58(17) | N(5)-C(17)-N(6) | 112.6(6) |

**Table S5.** Selected distances and angles for Zr-Et (**5**)

| | | | |
|---|---|---|---|
| **Distances (Å)** | | | |
| Zr(1)-C(25) | 2.3207(17) | Zr(2)-C(51) | 2.3154(15) |
| Zr(1)-N(1) | 2.2600(13) | Zr(2)-N(7) | 2.2552(13) |
| Zr(1)-N(2) | 2.2856(13) | Zr(2)-N(8) | 2.2956(12) |
| Zr(1)-N(3) | 2.2281(15) | Zr(2)-N(9) | 2.3221(14) |
| Zr(1)-N(4) | 2.3678(14) | Zr(2)-N(10) | 2.2422(13) |
| Zr(1)-N(5) | 2.3278(14) | Zr(2)-N(11) | 2.2278(13) |
| Zr(1)-N(6) | 2.2265(13) | Zr(2)-N(12) | 2.3468(13) |
| **Angles (°)** | | | |
| N(1)-Zr(1)-C(25) | 79.85(5) | N(7)-Zr(2)-C(51) | 81.14(5) |
| N(2)-Zr(1)-C(25) | 134.13(5) | N(8)-Zr(2)-C(51) | 134.57(5) |
| N(1)-Zr(1)-N(2) | 57.96(5) | N(7)-Zr(2)-N(8) | 57.67(5) |
| N(1)-C(1)-N(2) | 111.55(13) | N(7)-C(27)-N(8) | 110.85(12) |
| N(3)-Zr(1)-C(25) | 92.90(5) | N(9)-Zr(2)-C(51) | 79.39(5) |
| N(4)-Zr(1)-C(25) | 136.88(5) | N(10)-Zr(2)-C(51) | 105.78(5) |
| N(3)-Zr(1)-N(4) | 57.72(4) | N(9)-Zr(2)-N(10) | 58.31(5) |
| N(3)-C(9)-N(4) | 112.87(13) | N(9)-C(35)-N(10) | 113.24(13) |
| N(5)-Zr(1)-C(25) | 78.31(5) | N(11)-Zr(2)-C(51) | 90.77(5) |
| N(6)-Zr(1)-C(25) | 103.99(5) | N(12)-Zr(2)-C(51) | 134.53(5) |
| N(5)-Zr(1)-N(6) | 58.31(4) | N(11)-Zr(2)-N(12) | 58.07(4) |
| N(5)-C(17)-N(6) | 112.99(12) | N(11)-C(43)-N(12) | 113.27(12) |

**Table S6.** Selected distances and angles for Hf-Et (**6**)

| | | | |
|---|---|---|---|
| **Distances (Å)** | | | |
| Hf(1)-C(25) | 2.295(2) | Hf(2)-C(51) | 2.298(2) |
| Hf(1)-N(1) | 2.2379(18) | Hf(2)-N(7) | 2.2405(18) |
| Hf(1)-N(2) | 2.2831(17) | Hf(2)-N(8) | 2.2795(18) |
| Hf(1)-N(3) | 2.2057(17) | Hf(2)-N(9) | 2.2041(19) |
| Hf(1)-N(4) | 2.3305(18) | Hf(2)-N(10) | 2.3487(19) |
| Hf(1)-N(5) | 2.3072(18) | Hf(2)-N(11) | 2.3105(19) |
| Hf(1)-N(6) | 2.2831(17) | Hf(2)-N(12) | 2.2047(17) |
| **Angles (°)** | | | |
| N(1)-Hf(1)-C(25) | 81.50(7) | N(7)-Hf(2)-C(51) | 80.42(7) |
| N(2)-Hf(1)- C(25) | 135.50(7) | N(8)-Hf(2)-C(51) | 135.01(7) |
| N(1)-Hf(1)-N(2) | 57.93(6) | N(7)-Hf(2)-N(8) | 58.12(6) |
| N(1)-C(1)-N(2) | 110.80(17) | N(7)-C(27)-N(8) | 111.35(18) |
| N(3)-Hf(1)-C(25) | 91.12(7) | N(9)-Hf(2)-C(51) | 93.06(8) |
| N(4)-Hf(1)-C(25) | 134.68(7) | N(10)-Hf(2)-C(51) | 136.99(7) |
| N(3)-Hf(1)-N(4) | 58.58(6) | N(9)-Hf(2)-N(10) | 58.25(6) |
| N(3)-C(9)-N(4) | 113.36(18) | N(9)-C(35)-N(10) | 112.66(19) |
| N(5)-Hf(1)-C(25) | 79.20(7) | N(11)-Hf(2)-C(51) | 78.04(7) |
| N(6)-Hf(1)-C(25) | 105.19(7) | N(12)-Hf(2)-C(51) | 103.40(7) |
| N(5)-Hf(1)-N(6) | 58.63(6) | N(11)-Hf(2)-N(12) | 58.66(6) |
| N(5)-C(17)-N(6) | 113.05(18) | N(11)-C(43)-N(12) | 112.76(18) |

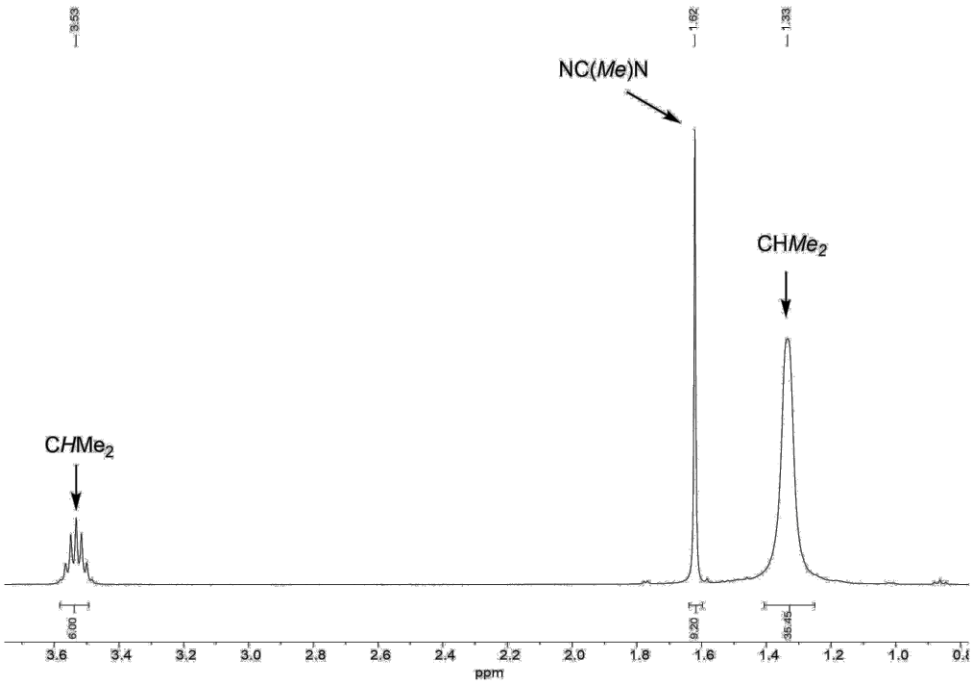


**Fig. S3.** $^{1}$H NMR spectrum of Zr-Cl (**1**) in benzene-$d_6$ at 23 °C.

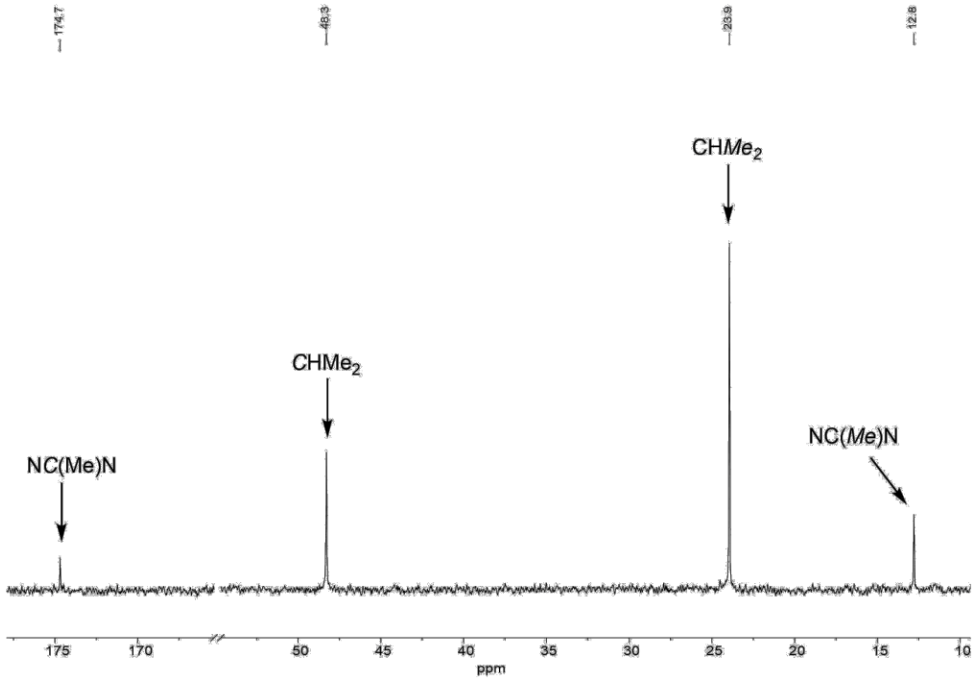


**Fig. S4.** $^{13}$C{$^{1}$H} NMR spectrum of Zr-Cl (**1**) in benzene-$d_6$ at 23 °C.

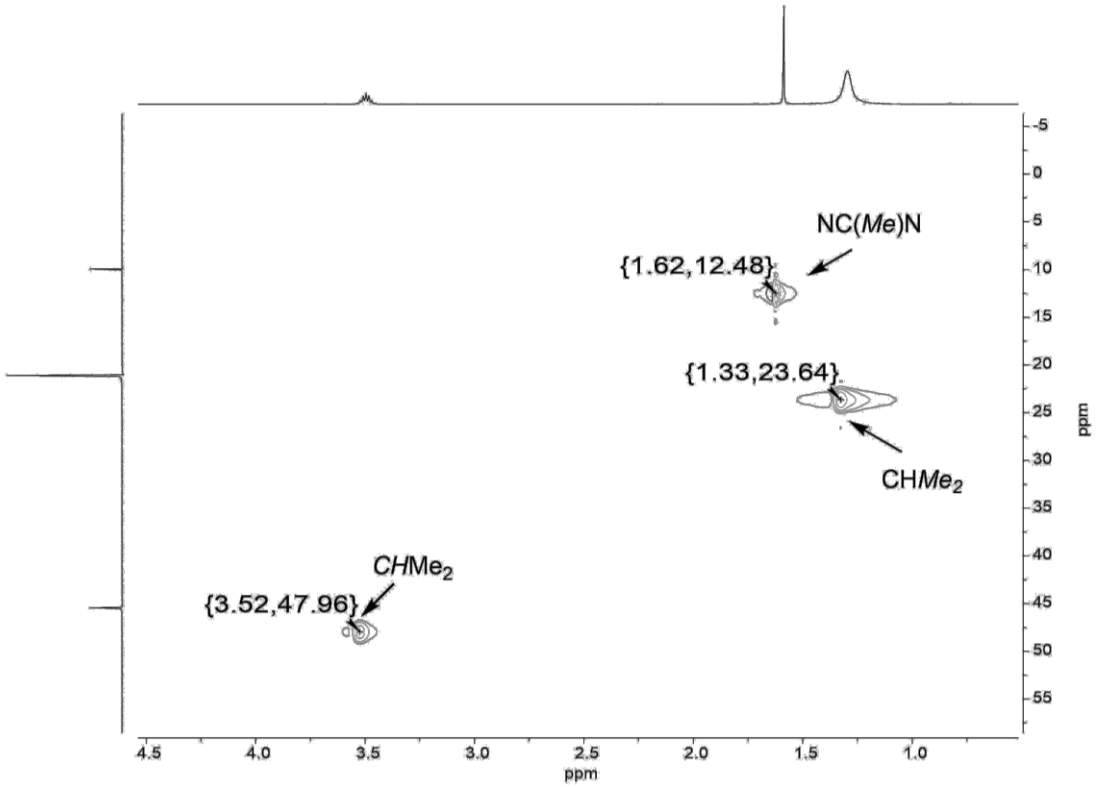


**Fig. S5.** $^{1}$H-$^{13}$C HSQC NMR spectrum of Zr-Cl (**1**) in benzene-$d_6$ at 23 °C.

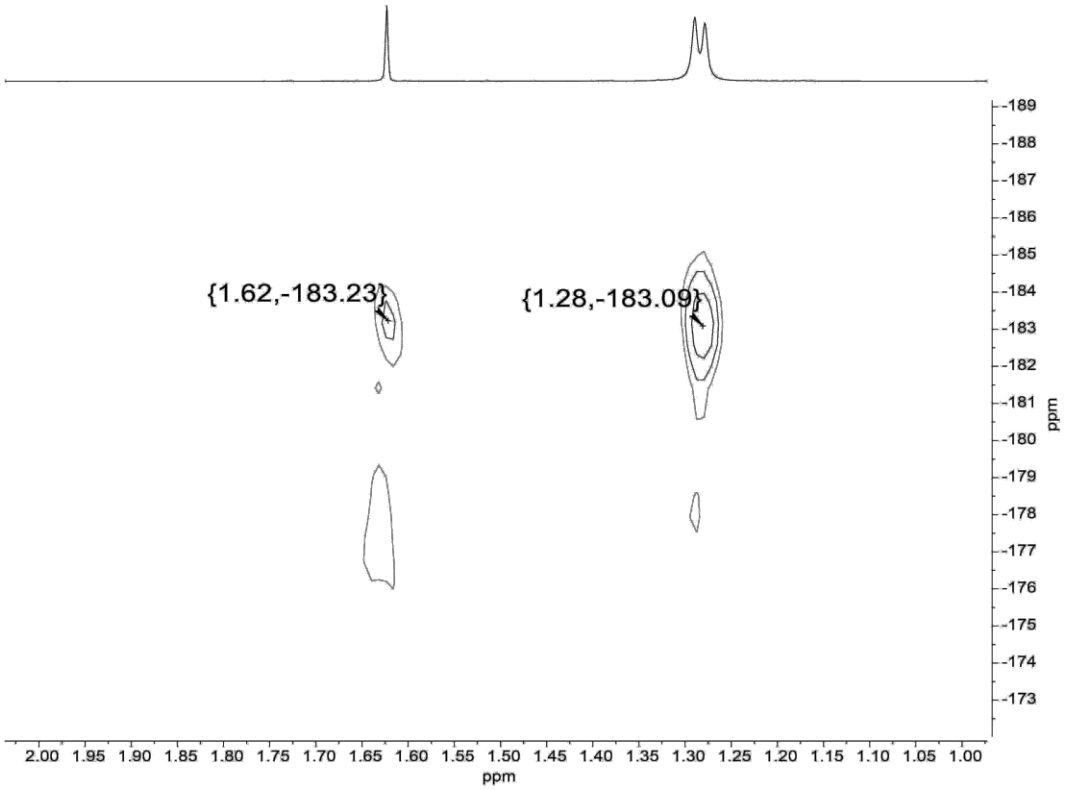


**Fig. S6.** $^{1}$H-$^{15}$N gHMBC NMR spectrum of Zr-Cl (**1**) in benzene-$d_6$ at 60 °C.

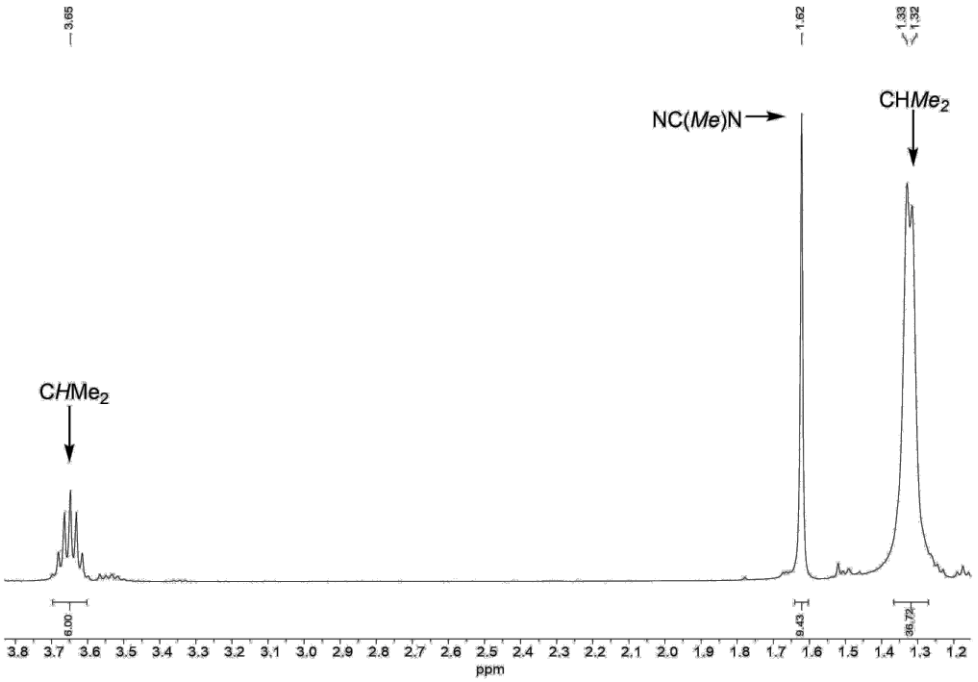


**Fig. S7.** $^{1}$H NMR spectrum of Hf-Cl (**2**) in benzene-$d_6$ at 23 °C.

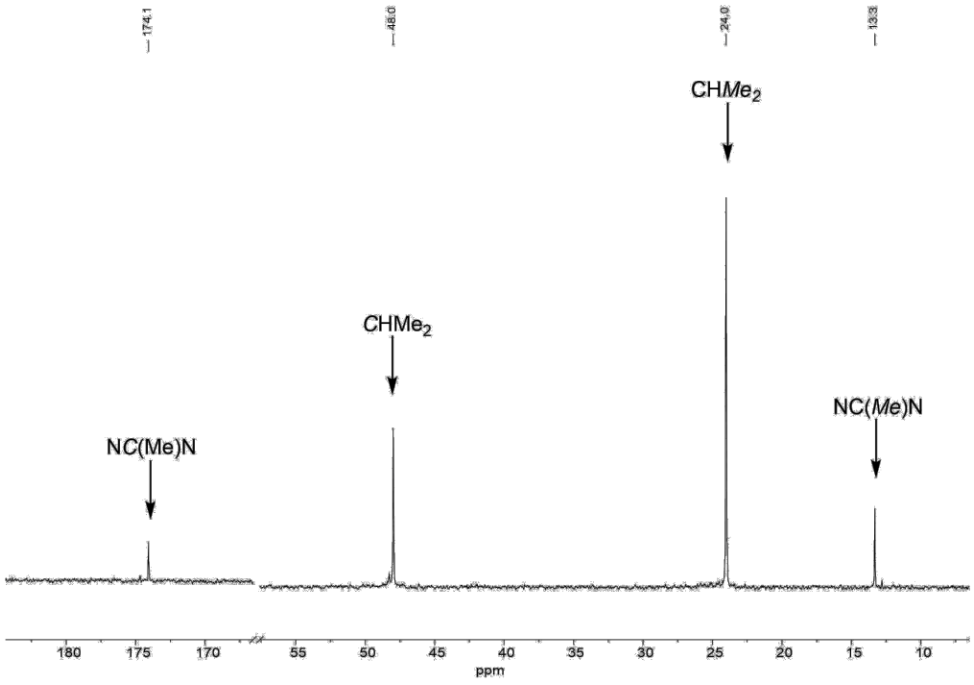


**Fig. S8.** $^{13}$C{$^{1}$H} NMR spectrum of Hf-Cl (**2**) in benzene-$d_6$ at 23 °C.

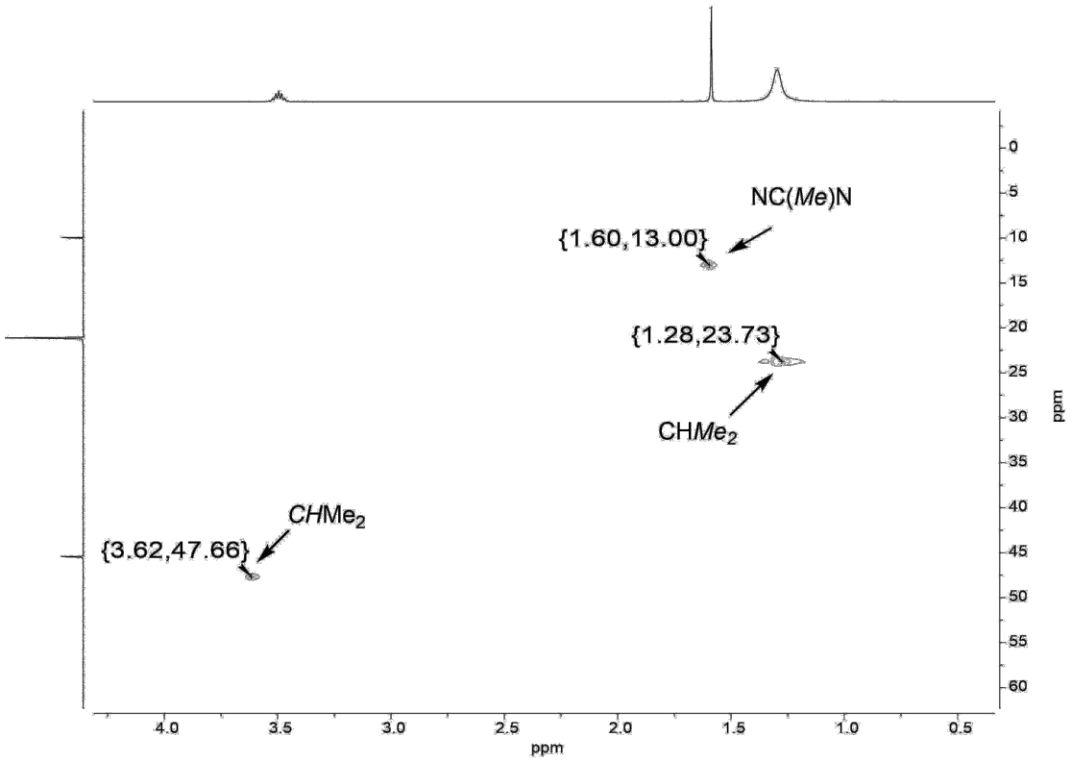


**Fig. S9**. $^{1}$H-$^{13}$C HSQC NMR spectrum of Hf-Cl (**2**) in benzene-$d_6$ at 23 °C.

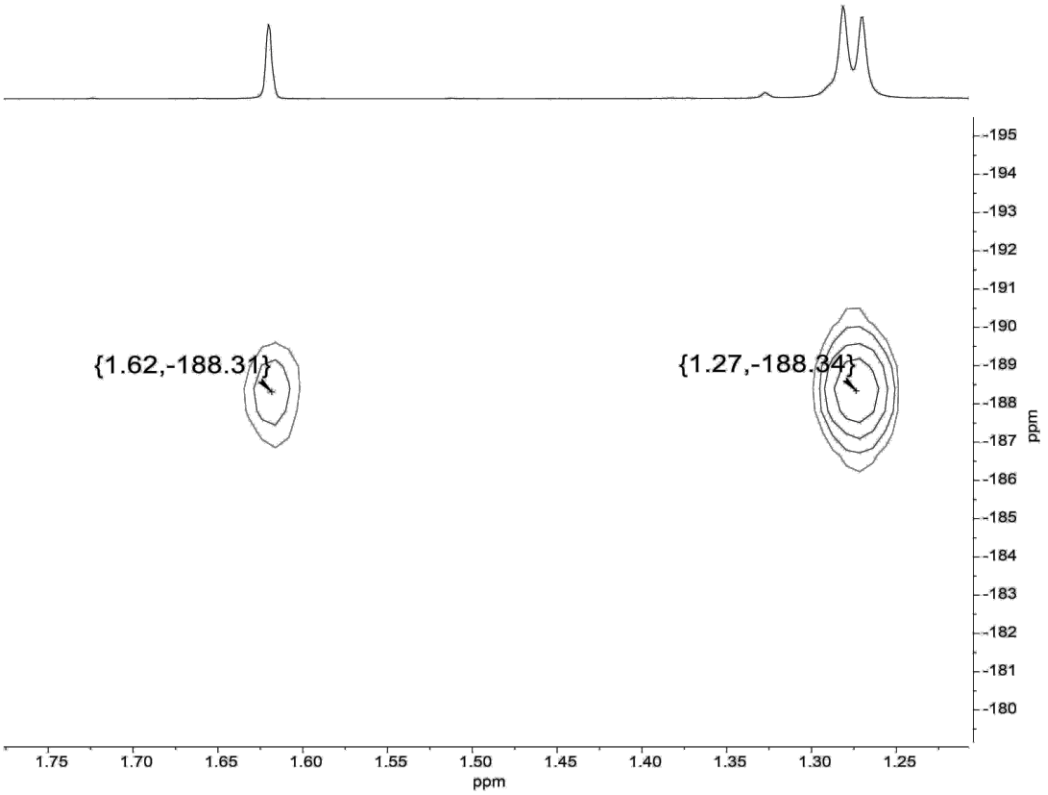


**Fig. S10.** $^{1}$H-$^{15}$N gHMBC NMR spectrum of Hf-Cl (**2**) in benzene-$d_6$ at 60 °C.

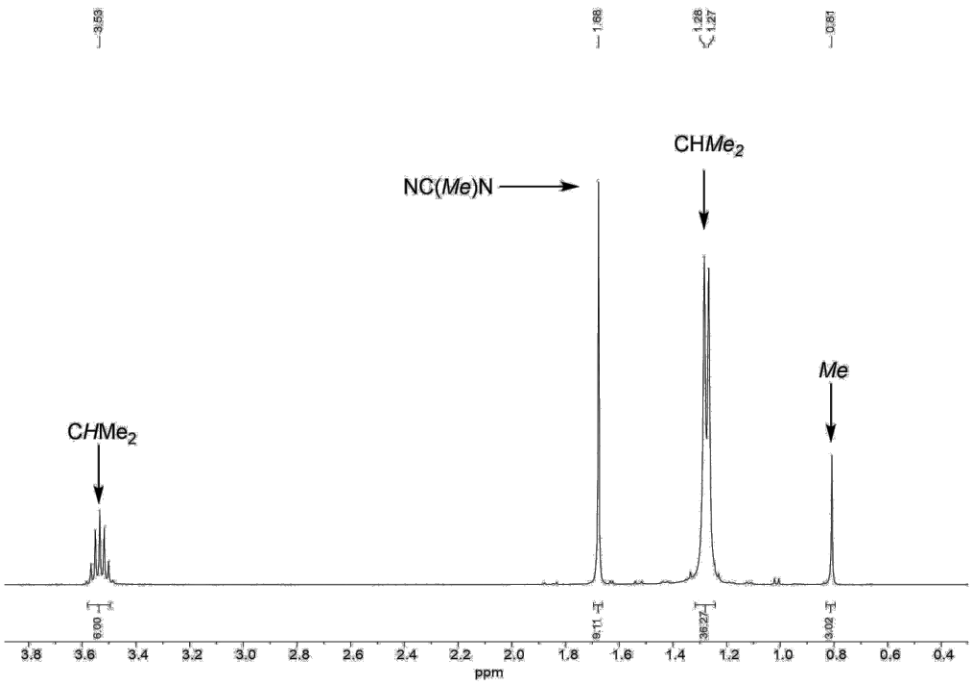


**Fig. S11.** $^{1}$H NMR spectrum of Zr-Me (**3**) in benzene-$d_6$ at 23 °C.

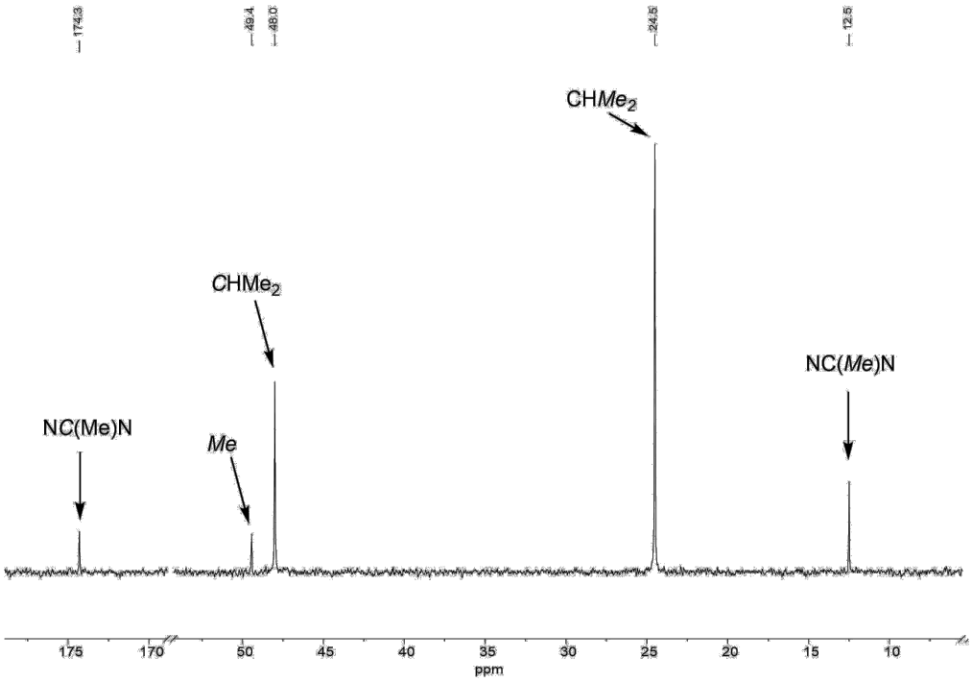


**Fig. S12.** $^{13}$C{$^{1}$H} NMR spectrum of Zr-Me (**3**) in benzene-$d_6$ at 23 °C.

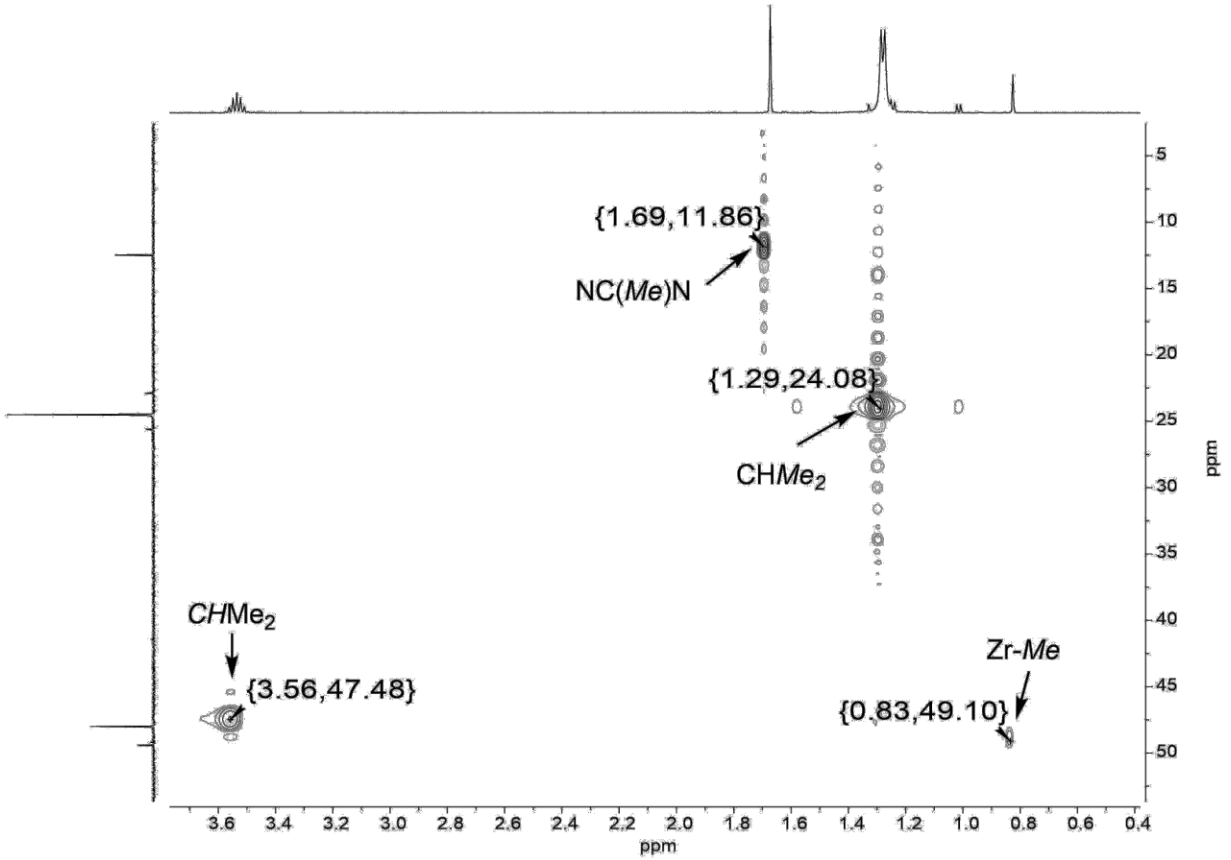


**Fig. S13.** $^{1}H$-$^{13}C$ HSQC NMR spectrum of Zr-Me (**3**) in benzene-$d_6$ at 23 °C.

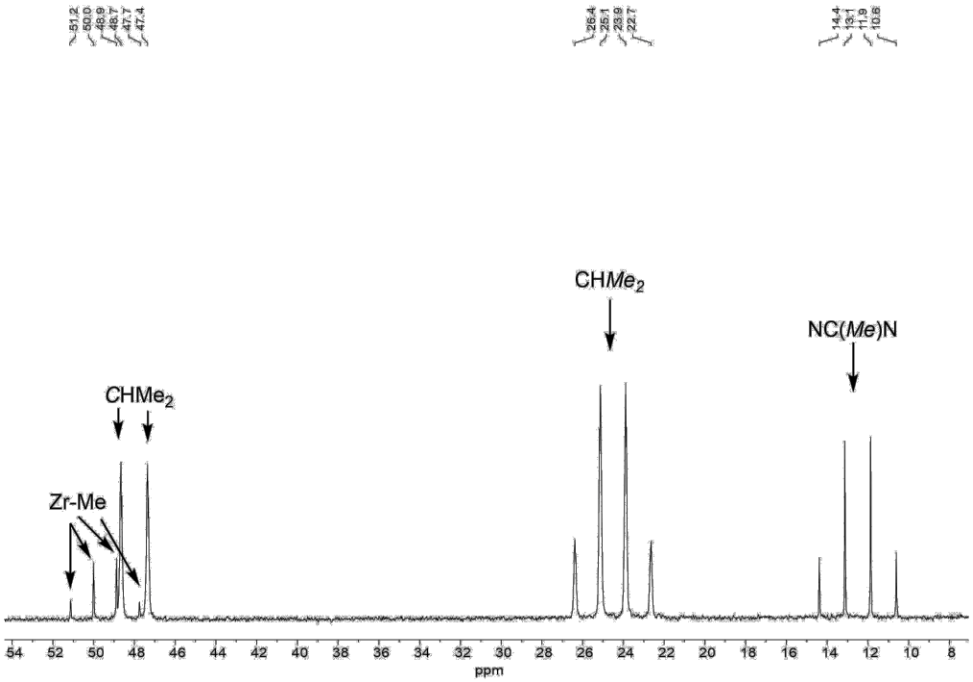


**Fig. S14.** Gated $^{13}C\{^{1}H\}$ NMR spectrum of Zr-Me (**3**) in benzene-$d_6$ at 23 °C.

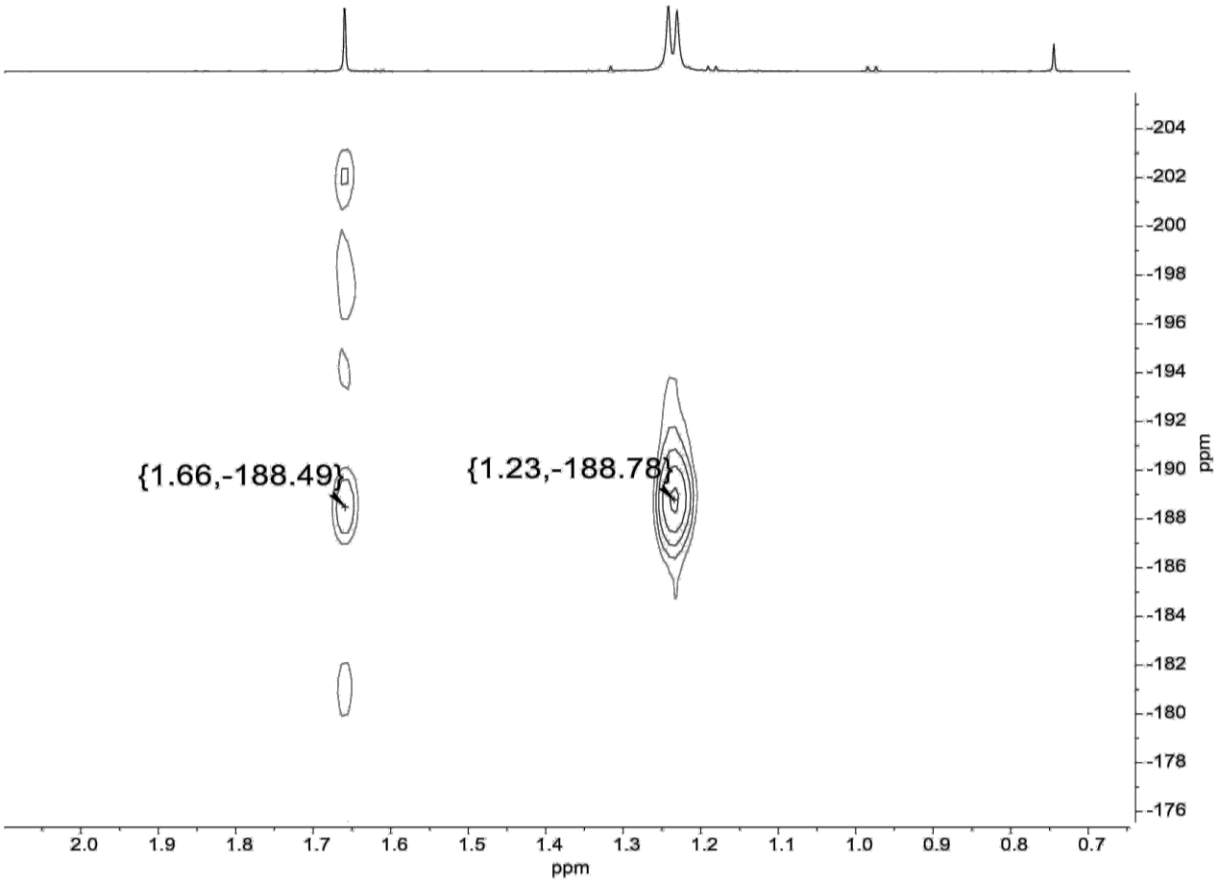


**Fig. S15.** $^{1}$H-$^{15}$N gHMBC NMR spectrum of Zr-Me (**3**) in benzene-$d_6$ at 45 °C.

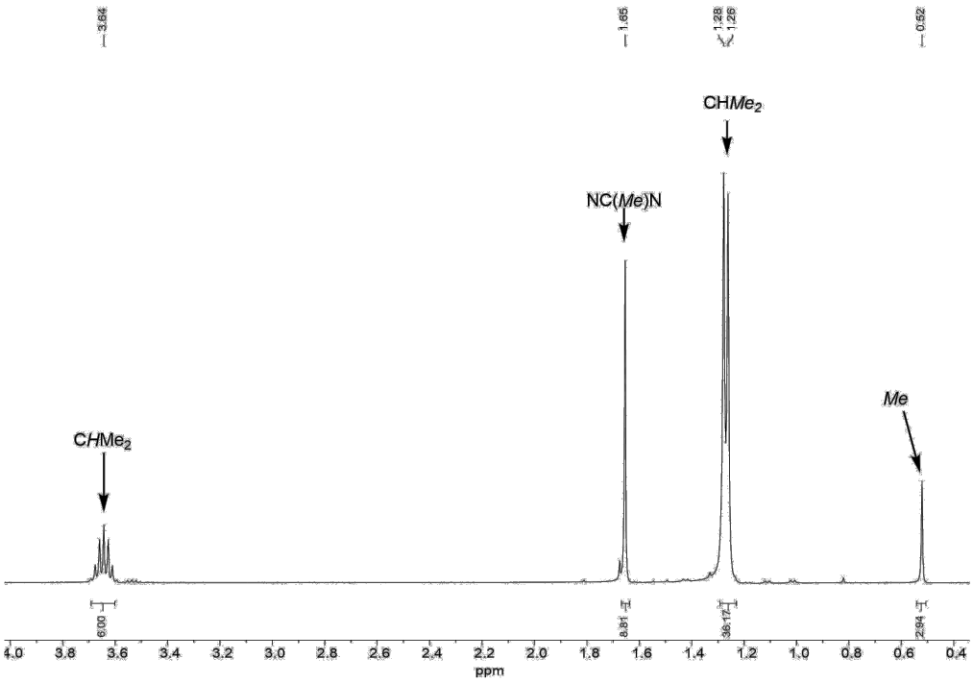


**Fig. S16.** $^{1}$H NMR spectrum of Hf-Me (**4**) in benzene-$d_6$ at 23 °C.

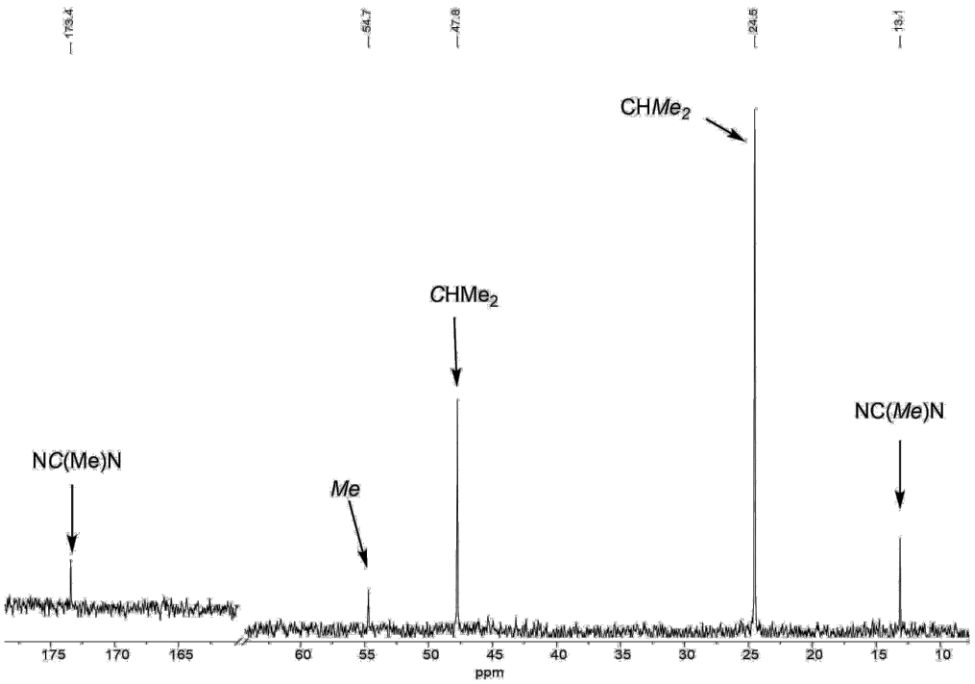


**Fig. S17.** $^{13}C\{^{1}H\}$ NMR spectrum of Hf-Me (**4**) in benzene-$d_6$ at 23 °C.

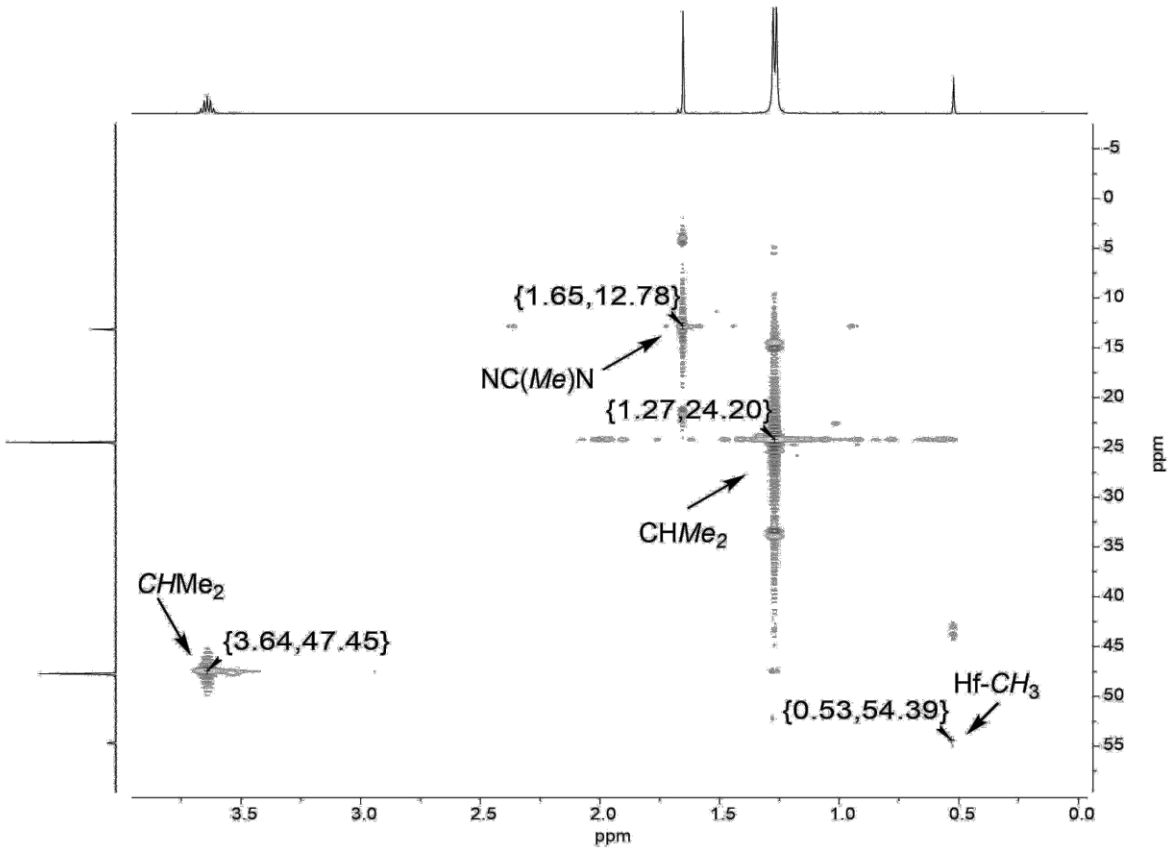


**Fig. S18.** $^{1}H$-$^{13}C$ HSQC NMR spectrum of Hf-Me (**4**) in benzene-$d_6$ at 23 °C.

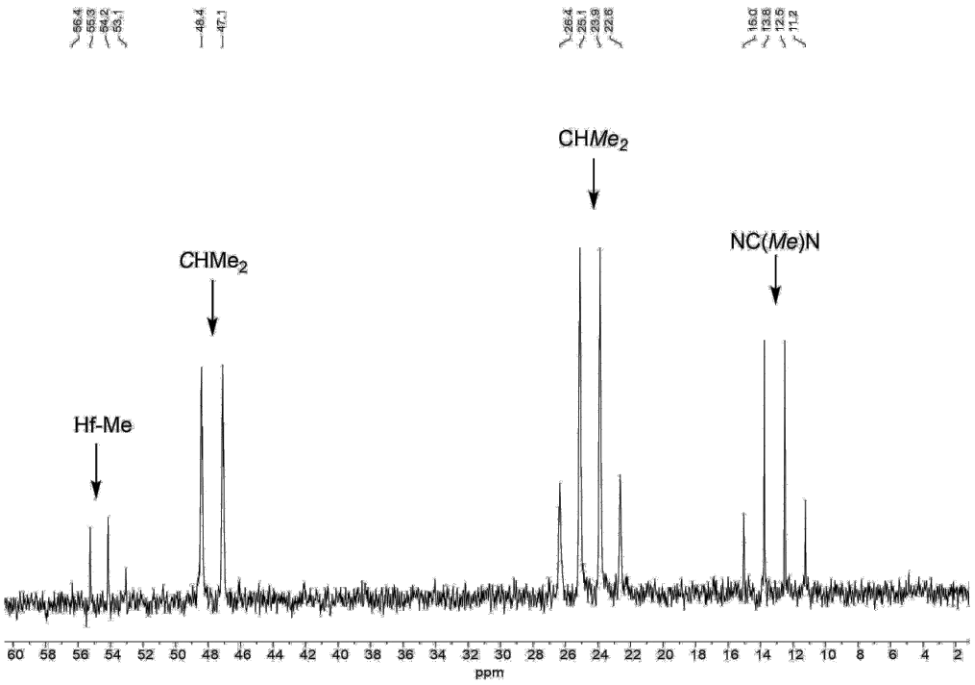


**Fig. S19.** Gated $^{13}C$ NMR spectrum of Hf-Me (**4**) in benzene-$d_6$ at 23 °C.

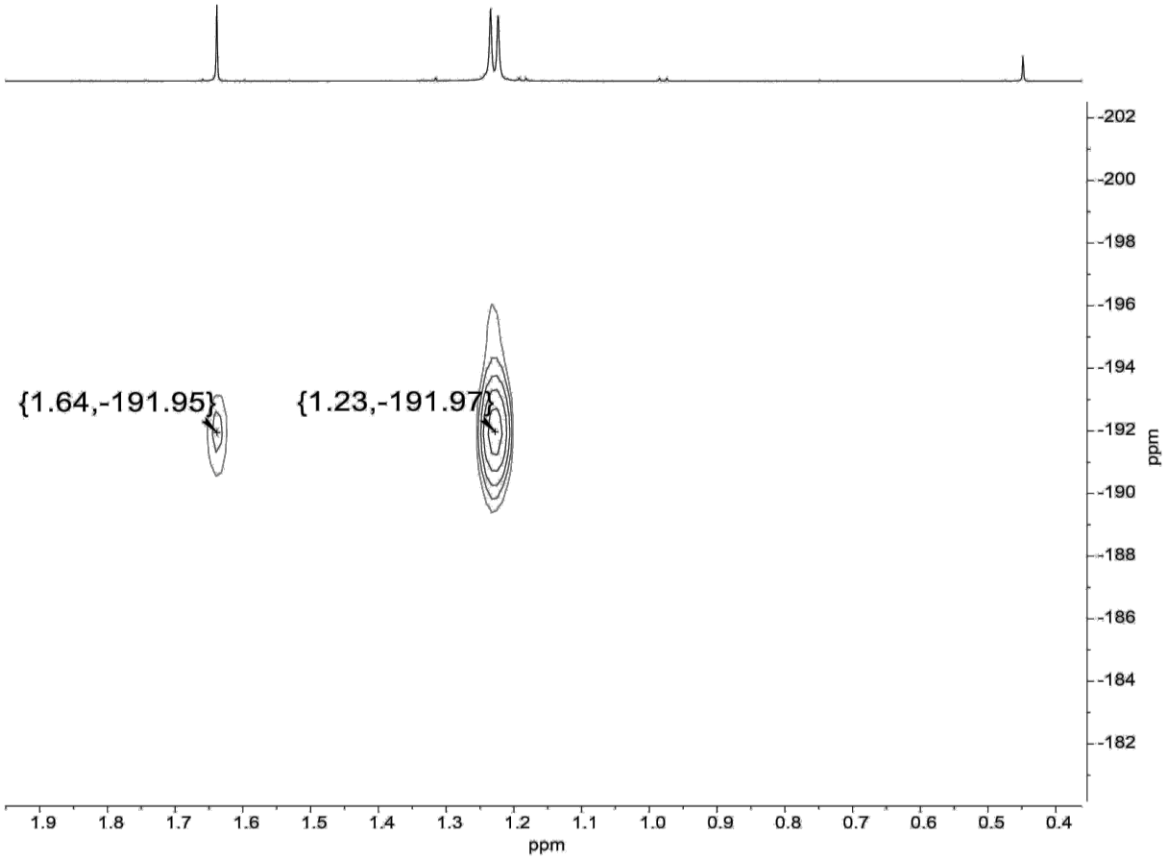


**Fig. S20.** $^{1}H$-$^{15}N$ gHMBC NMR spectrum of Hf-Me (**4**) in benzene-$d_6$ at 45 °C.

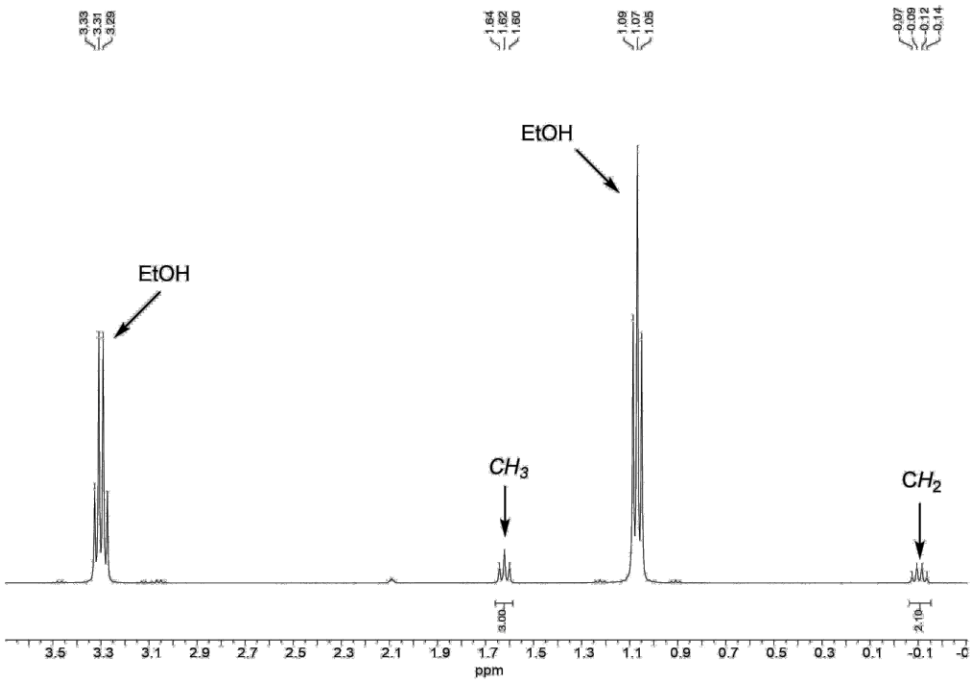


**Fig. S21.** Partial $^{1}$H NMR spectrum of EtMgCl in a benzene/$Et_2O$ solution in toluene-$d_8$ at 23 °C.

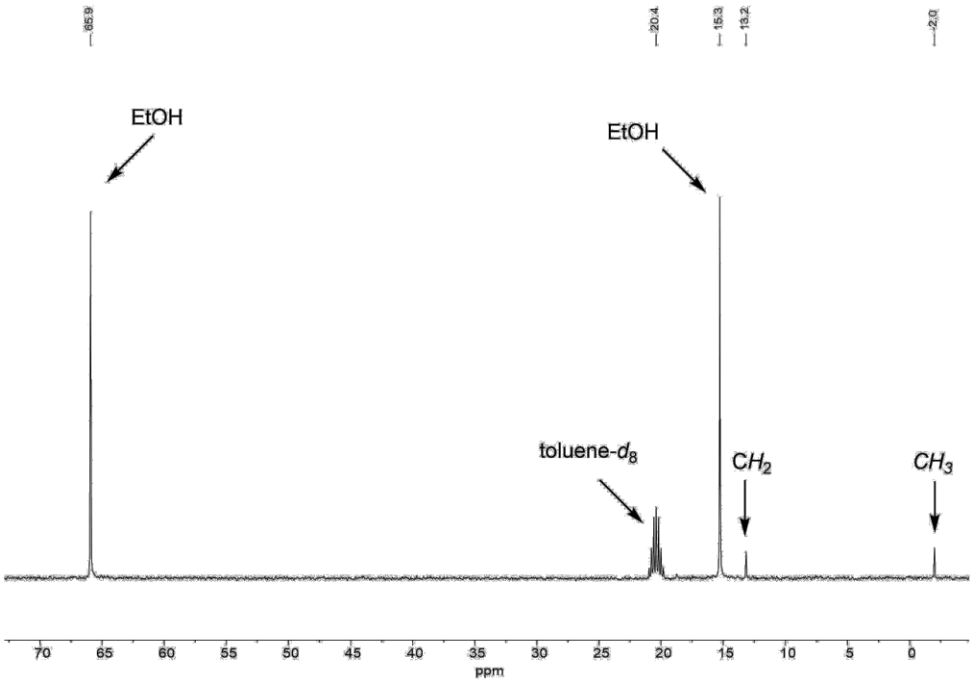


**Fig. S22.** Partial $^{13}C\{^{1}H\}$ NMR spectrum of EtMgCl in a benzene/$Et_2O$ solution in toluene-$d_8$ at 23 °C.

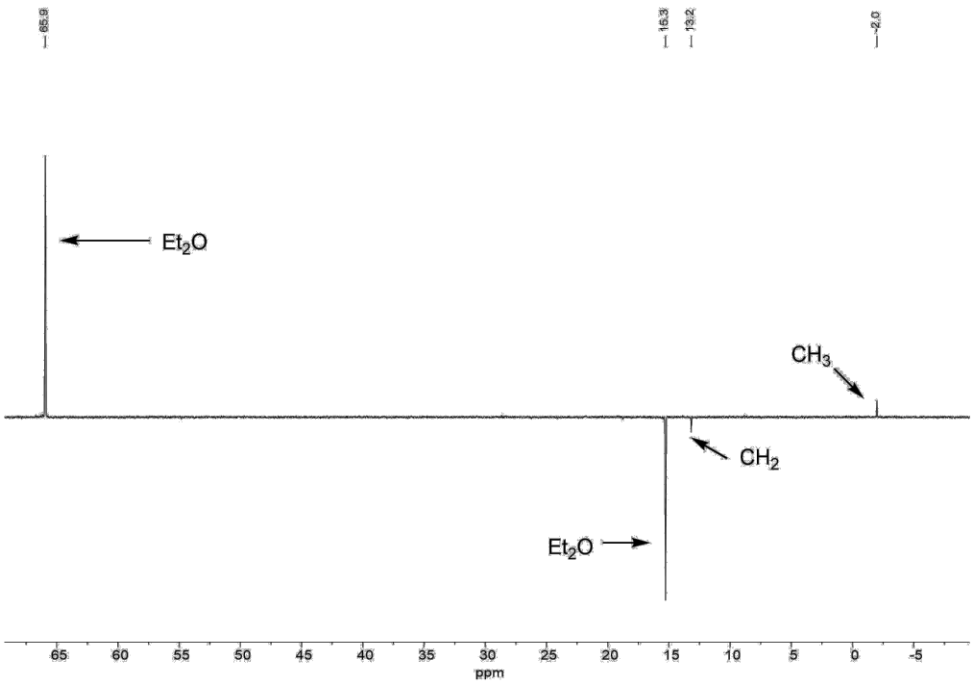


**Fig. S23.** DEPT-135 NMR spectrum of EtMgCl in a benzene/$Et_2O$ solution in toluene-$d_8$ at 23 °C.

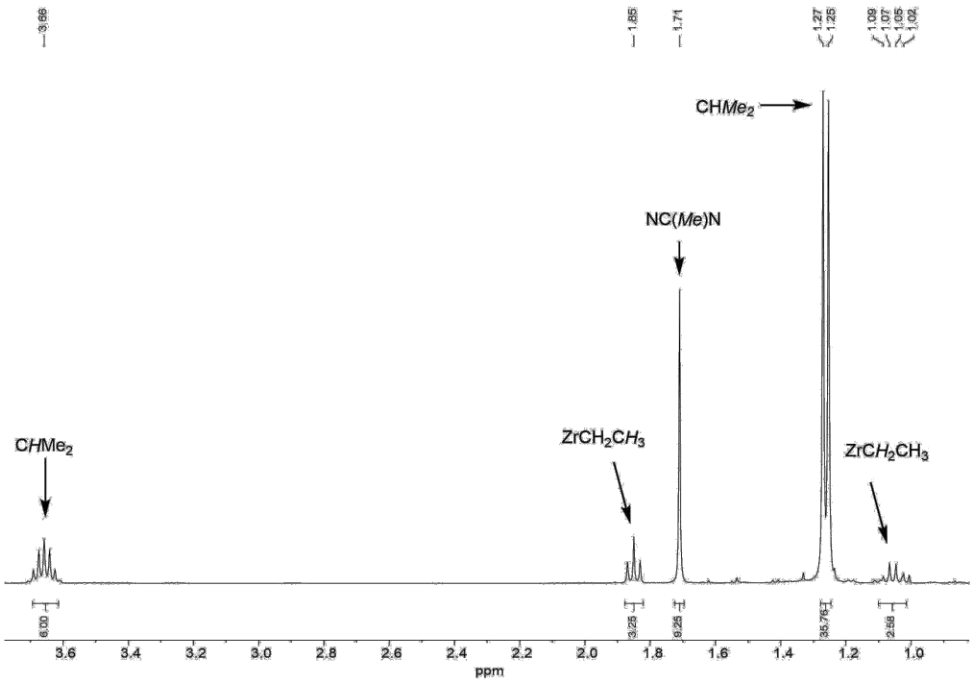


**Fig. S24.** $^1H$ NMR spectrum of Zr-Et (**5**) in benzene-$d_6$ at 23 °C.

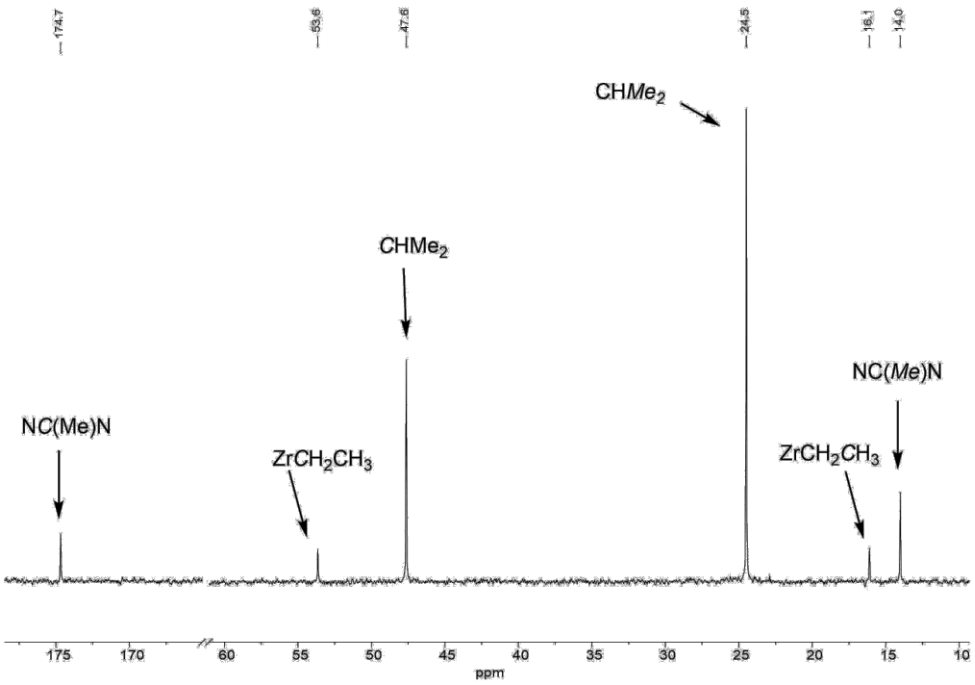


**Fig. S25.** $^{13}C\{^{1}H\}$ NMR spectrum of Zr-Et (**5**) in benzene-$d_6$ at 23 °C.

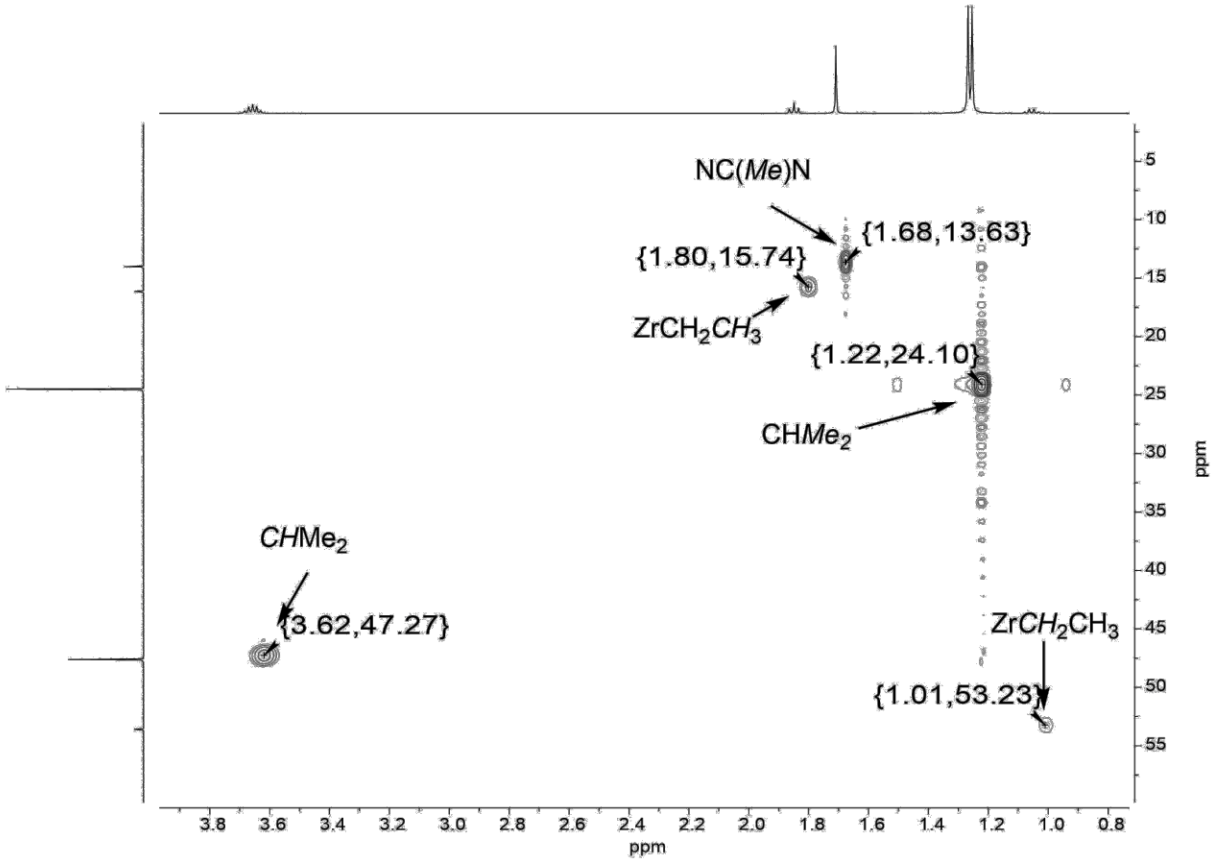


**Fig. S26.** $^{1}H$-$^{13}C$ HSQC NMR spectrum of Zr-Et (**5**) in benzene-$d_6$ at 23 °C.

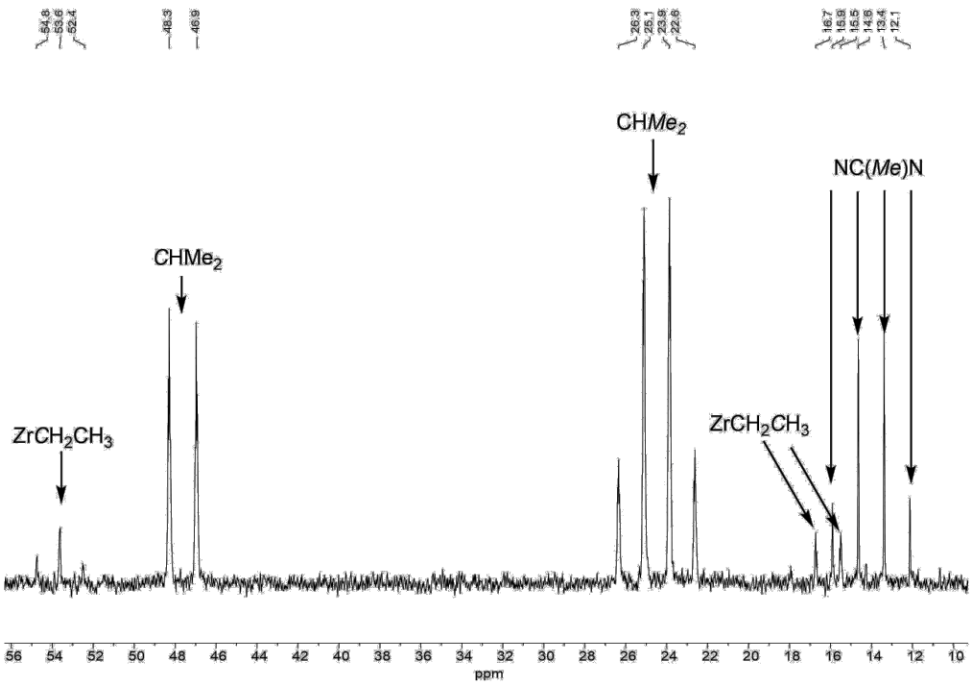


**Fig. S27.** Gated $^{13}C$ NMR spectrum of Zr-Et (**5**) in benzene-$d_6$ at 23 °C.

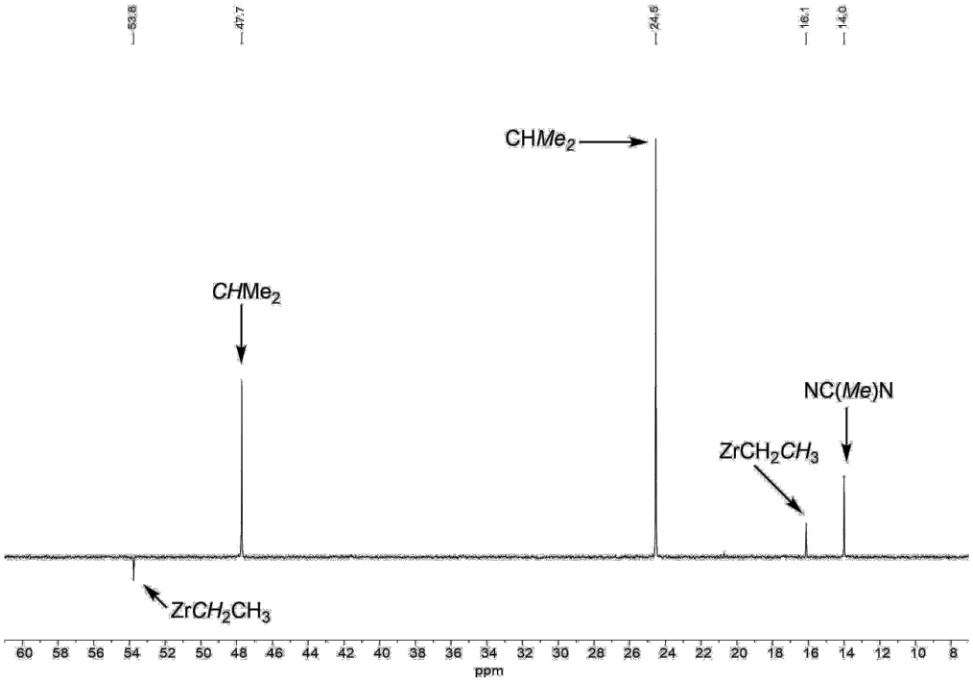


**Fig. S28.** DEPT-135 NMR spectrum of Zr-Et (**5**) in toluene-$d_8$ at 23 °C.

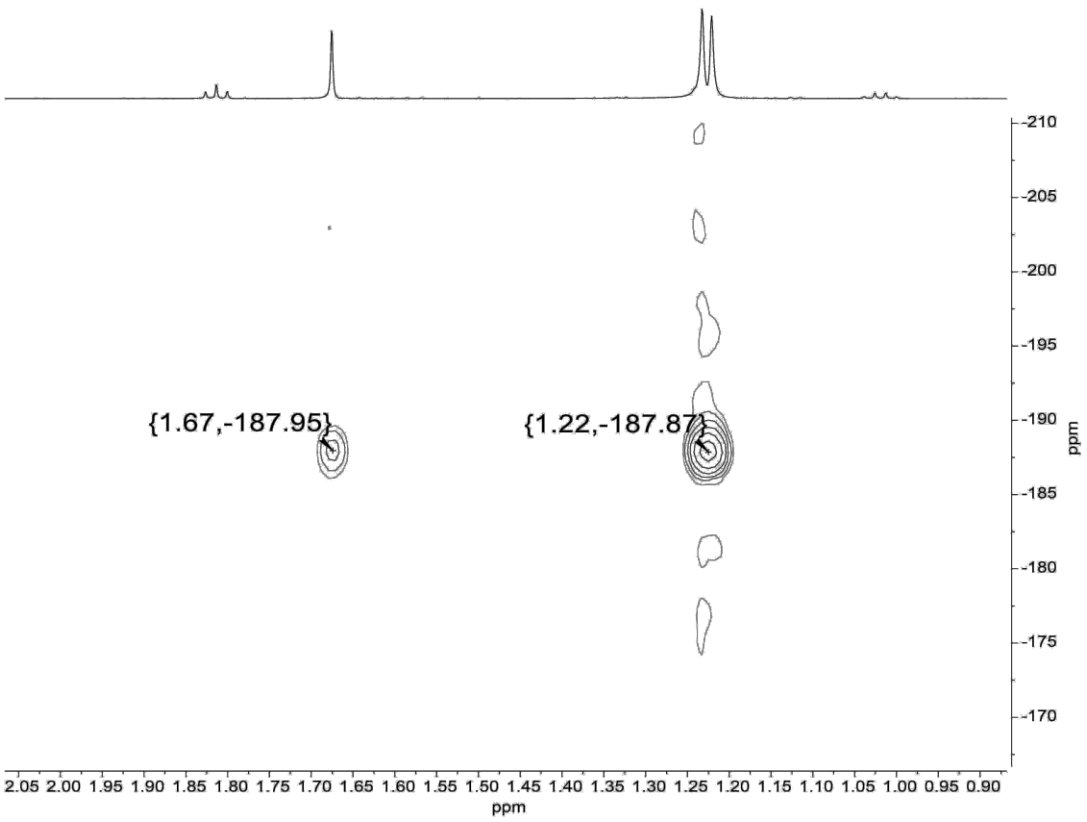


**Fig. S29.** $^{1}H$-$^{15}N$ gHMBC NMR spectrum of Zr-Et (**5**) in benzene-$d_6$ at 25 °C.

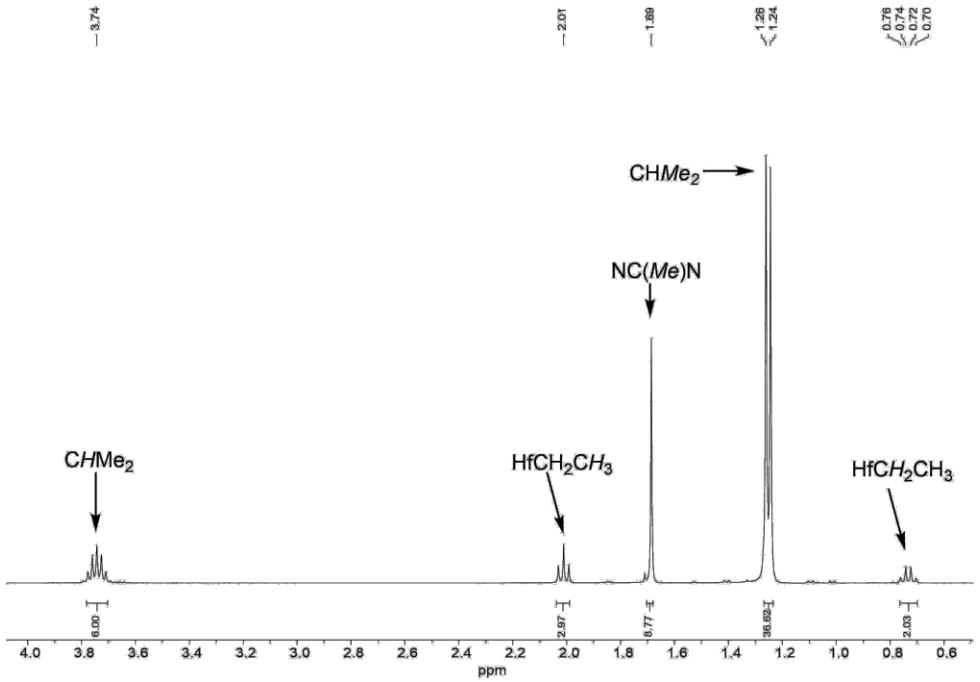


**Fig. S30.** $^{1}H$ NMR spectrum of Hf-Et (**6**) in benzene-$d_6$ at 23 °C.

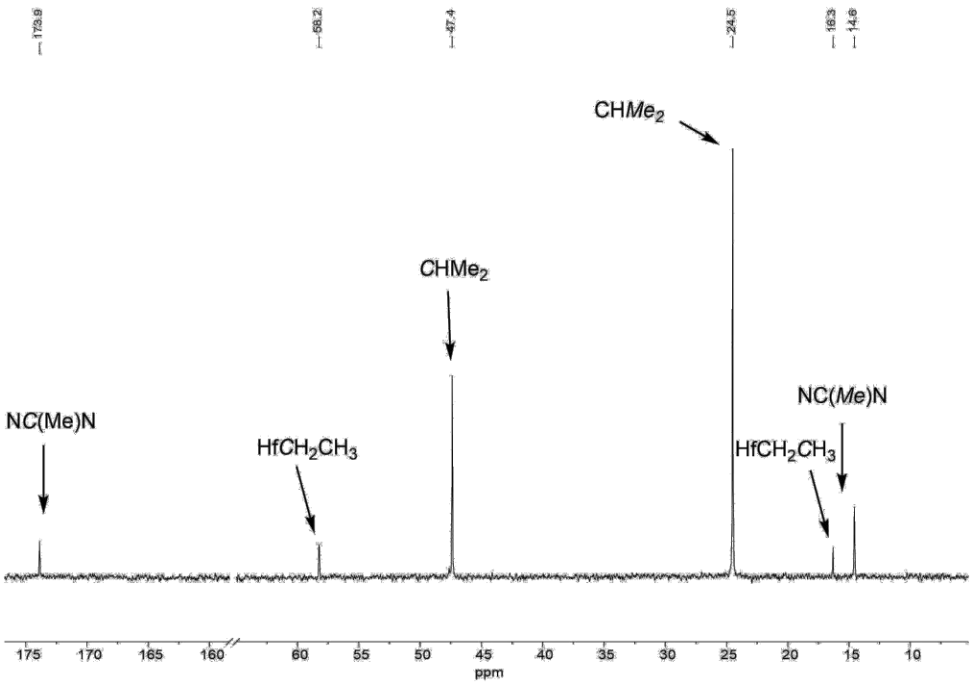


**Fig. S31.** $^{13}C\{^{1}H\}$ NMR spectrum of Hf-Et (**6**) in benzene-$d_6$ at 23 °C.

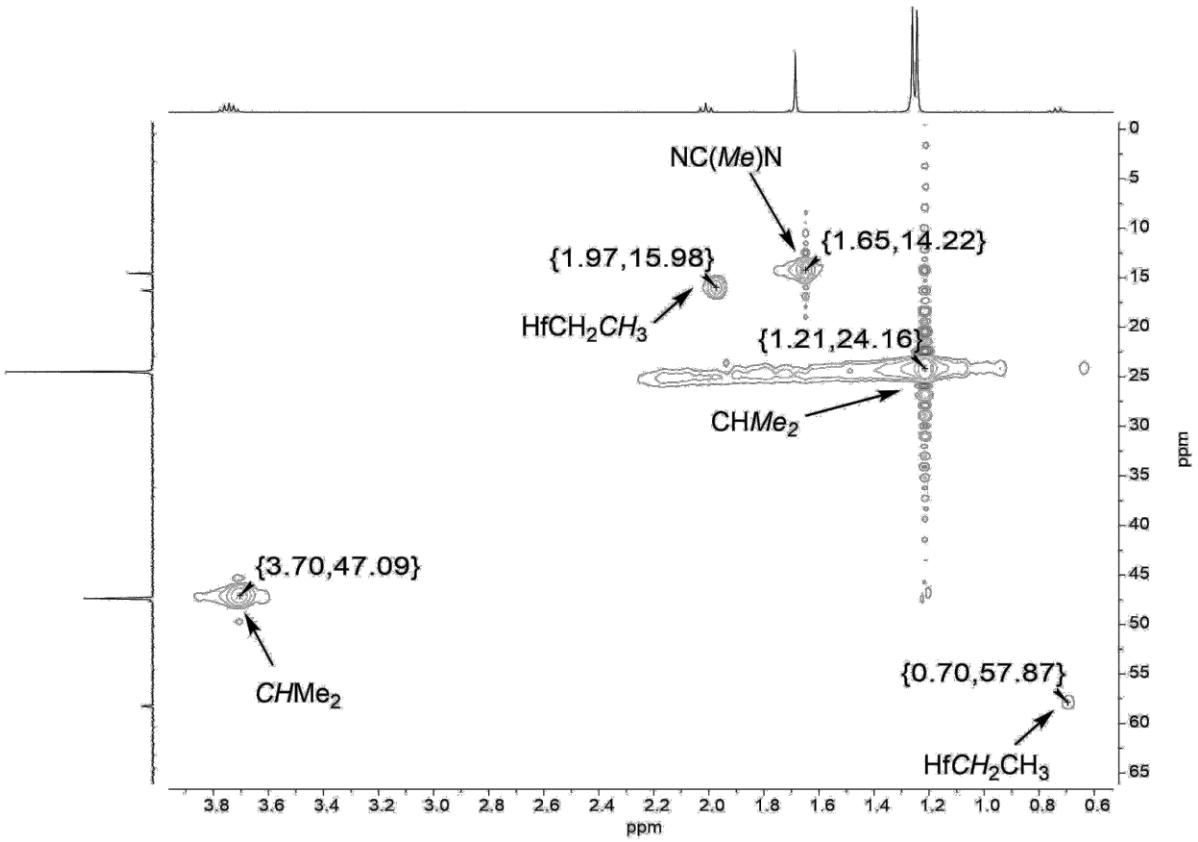


**Fig. S32.** $^{1}H$-$^{13}C$ HSQC NMR spectrum of Hf-Et (**6**) in benzene-$d_6$ at 23 °C.

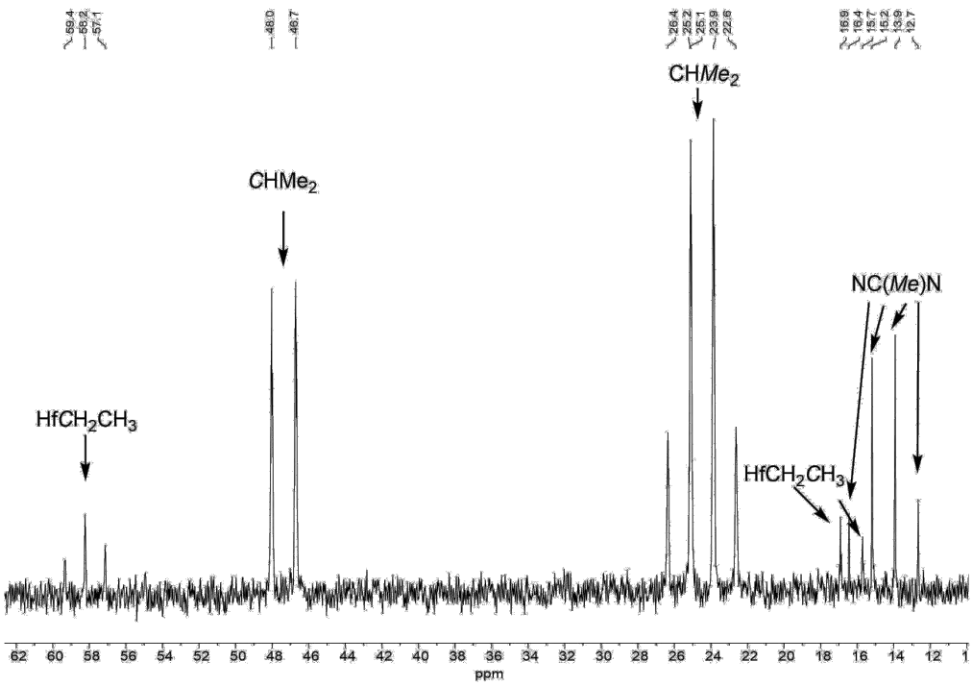


**Fig. S33.** Gated $^{13}C\{^{1}H\}$ NMR spectrum of Hf-Et (**6**) in benzene-$d_6$ at 23 °C.

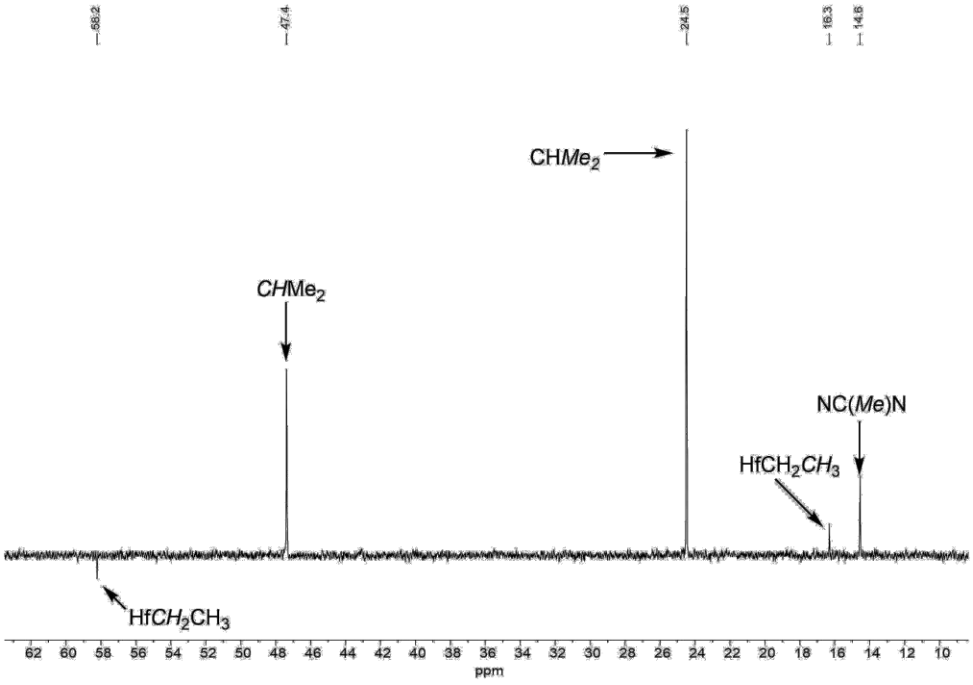


**Fig. S34**. DEPT-135 NMR spectrum of Hf-Et (**6**) in benzene-$d_6$ at 23 °C.

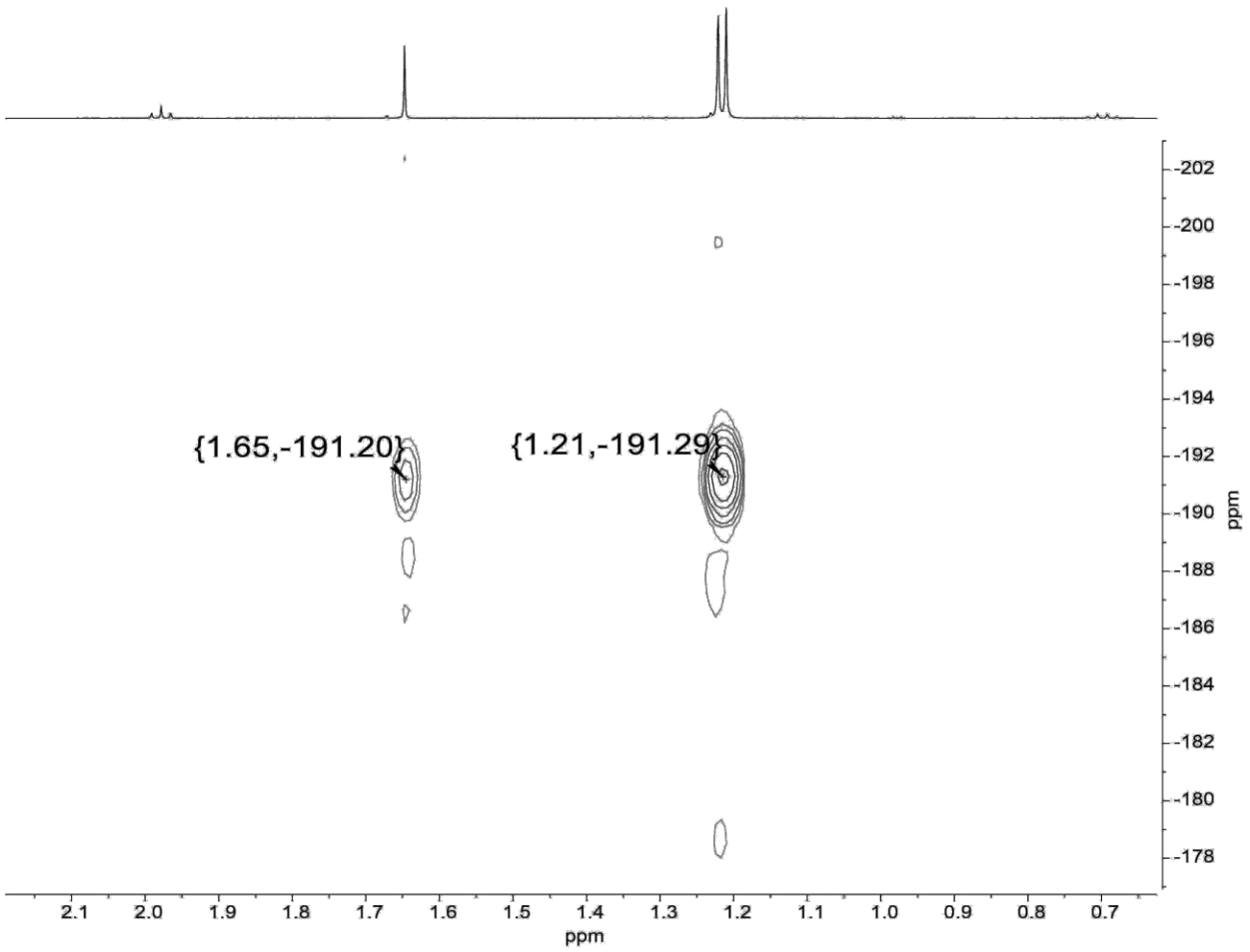


**Fig. S35.** $^{1}H$-$^{15}N$ gHMBC NMR spectrum of Hf-Et (**6**) in benzene-$d_6$ at 25 °C.

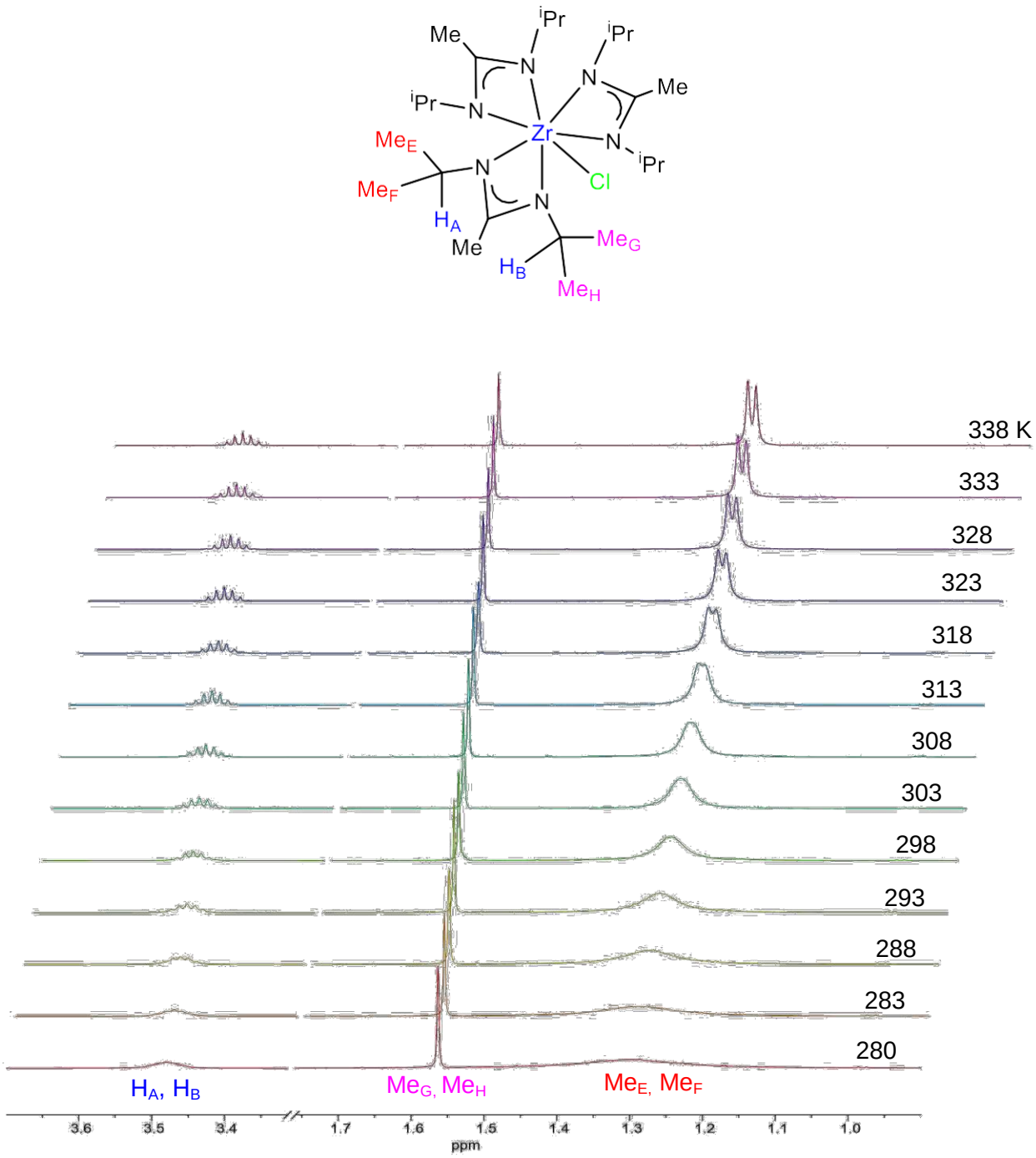


**Fig. S36**. Partial $^{1}$H NMR spectra of Zr-Cl (**1**) in benzene-$d_6$ at several temperatures recorded on a 500 MHz NMR spectrometer.

**Table S7.** Rate constants of the interconversions in Zr-Cl (**1**)

| ***T*** **(K)** | ***k*** **(s$^{-1}$) for** ***H*$_A$*H*$_B$**[b] | ***k*** **(s$^{-1}$) for** ***Me*$_E$*Me*$_F$** | ***k*** **(s$^{-1}$) for** ***Me*$_G$*Me*$_H$** | ***k*** **(s$^{-1}$) for** ***Me*$_{E-F}$*Me*$_{G-H}$** |
|---|---|---|---|---|
| 203(1) | | 7.86(7) | | |
| 208(1) | | 10.7(4) | 28.0(1) | |
| 213(1) | | 14.51(7) | 37.4(7) | |
| 218(1) | | 18.3(4) | 48(2) | |
| 223(1) | | 25.2(6) | 55(1) | |
| 228(1) | 131(2) | 34(1) | 69(3) | |
| 233(1) | 143(3) | 46(1) | 84.8(2) | |
| 238(1) | 154(3) | 52.3(9) | 112(5) | 297.9(6) |
| 243(1) | 177(3) | | 152(2) | 333(3) |
| 248(1) | 211(6) | | | 365(16) |
| 253(1) | 249(5) | | | 431(8) |
| 258(1) | 279(1) | | | 482(11) |
| 263(1) | 301(1) | | | 573(15) |
| 268(1) | | | | 688(3) |
| 273(1) | | | | 745(3) |

[a] The total uncertainties $\delta k/k$ were calculated from $\delta k_{ran}/k$ from each column and $\delta k_{sys}/k$ = 0.050. (1) *H*$_A$*H*$_B$: $\delta k_{ran}/k$ = 0.027, $\delta k/k$ = 0.057; (2) *Me*$_E$*Me*$_F$: $\delta k_{ran}/k$ = 0.039, $\delta k/k$ = 0.063; (3) *Me*$_G$*Me*$_H$: $\delta k_{ran}/k$ = 0.045, $\delta k/k$ = 0.067; (4) *Me*$_{E-F}$*Me*$_{G-H}$: $\delta k_{ran}/k$ = 0.043, $\delta k/k$ = 0.066.

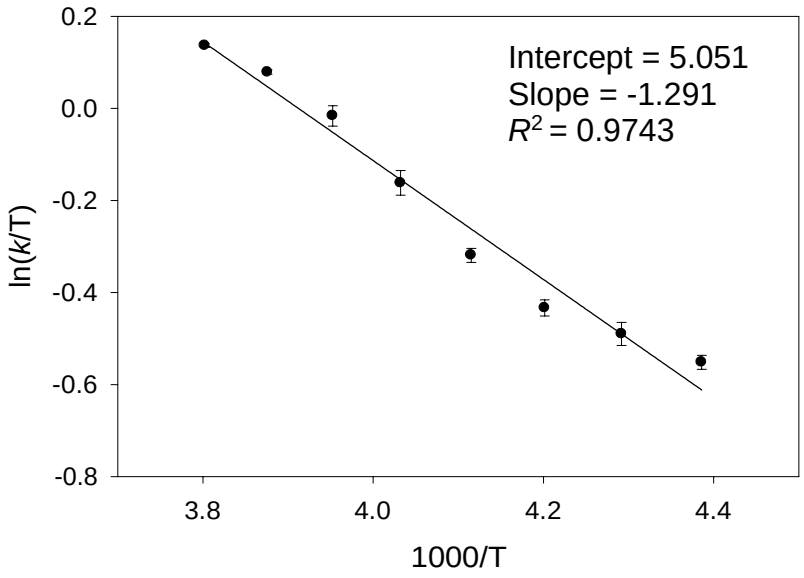


**Fig. S37.** Eyring plot of the $H_AH_B$ exchange in Zr-Cl (**1**) yielding activation parameters for the exchange.

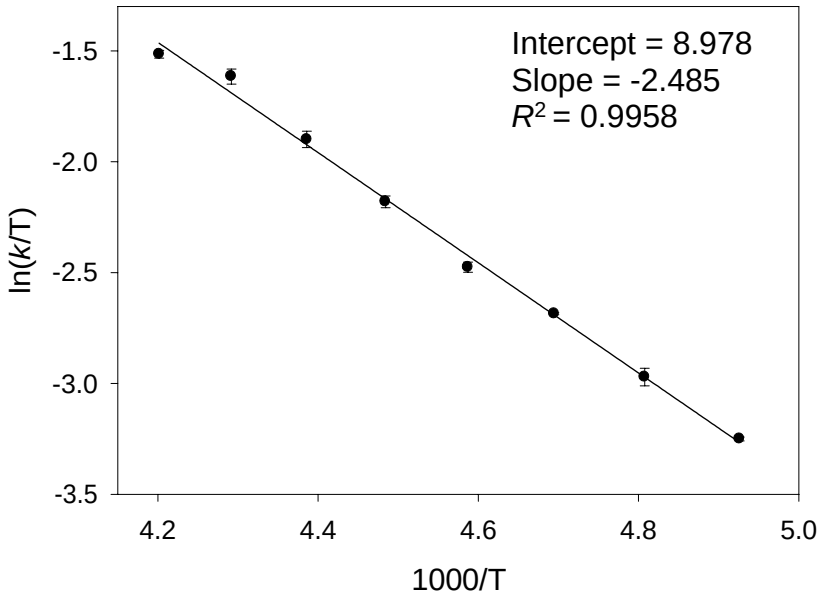


**Fig. S38.** Eyring plot of the $Me_EMe_F$ exchange in Zr-Cl (**1**) yielding activation parameters for the exchange.

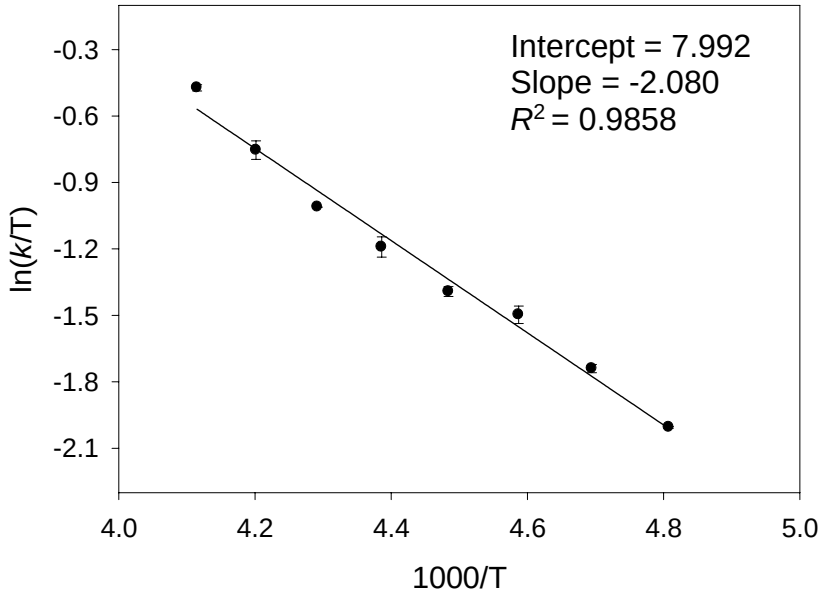


**Fig. S39.** Eyring plot of the $Me_GMe_H$ exchange in Zr-Cl (**1**) yielding activation parameters for the exchange.

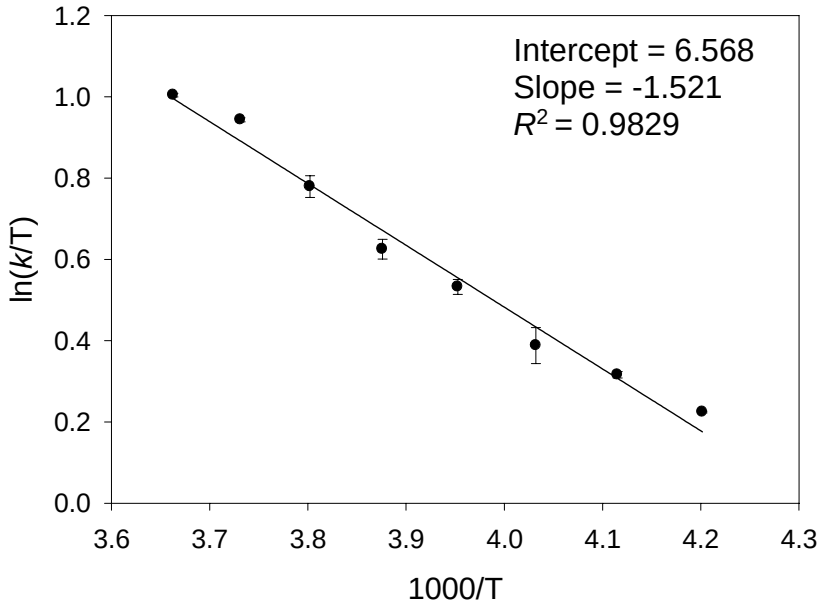


**Fig. S40.** Eyring plot of the $Me_{E\text{-}F}Me_{G\text{-}H}$ exchange in Zr-Cl (**1**) yielding activation parameters for the exchange.

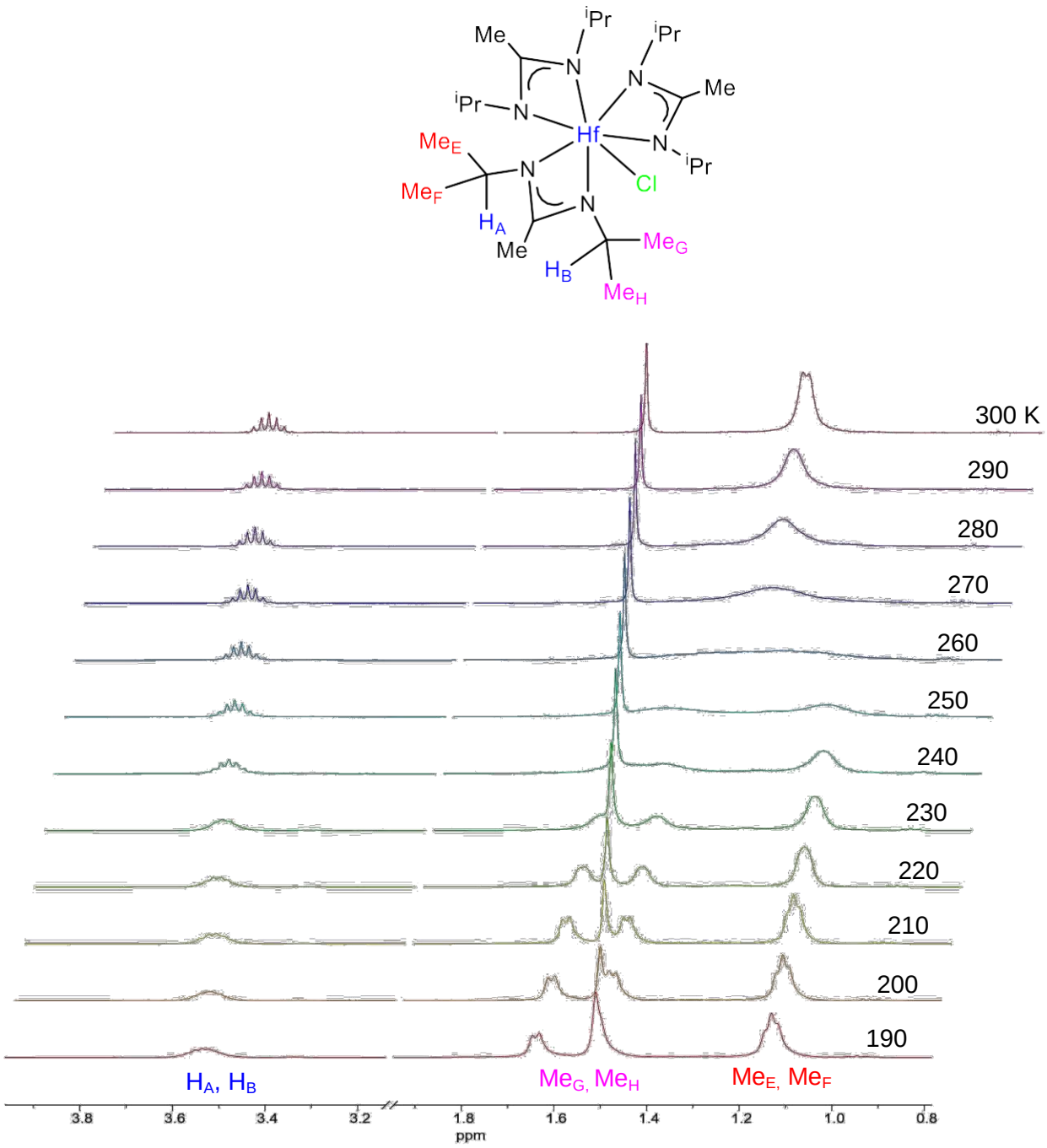


**Fig. S41.** Partial $^{1}$H NMR spectra of Hf-Cl (**2**) at several temperatures in toluene-$d_8$ recorded on a 400 MHz NMR spectrometer.

**Table S8.** Rate constants for the interconversions in Hf-Cl (**2**)

| ***T*** **(K)** | ***k*** **(s$^{-1}$) for *Me*$_E$*Me*$_F$** | ***k*** **(s$^{-1}$) for *Me*$_G$*Me*$_H$** | ***k*** **(s$^{-1}$) for *Me*$_{E\text{-}F}$*Me*$_{G\text{-}H}$** |
|---|---|---|---|
| 200(1) | 7.4(1) | | |
| 205(1) | 8.44(4) | | |
| 210(1) | 10.54(0) | | |
| 215(1) | 13.0(2) | 51.3(9) | |
| 220(1) | 15.0(4) | 61(3) | |
| 225(1) | 16.9(5) | 76.9(6) | |
| 230(1) | 20.3(5) | 102(2) | 287(6) |
| 235(1) | 26.01(0) | 141(6) | 318.4(6) |
| 240(1) | | 169(5) | 373(2) |
| 245(1) | | 222.0(6) | 425(13) |
| 250(1) | | 236.6(7) | 485(18) |
| 255(1) | | | 610(17) |
| 260(1) | | | 702(6) |
| 265(1) | | | 765(6) |

[a] The total uncertainties $\delta k/k$ were calculated from $\delta k_{ran}/k$ from each column and $\delta k_{sys}/k$ = 0.050. (1) *Me*$_E$*Me*$_F$: $\delta k_{ran}/k$ = 0.029, $\delta k/k$ = 0.058; (2) *Me*$_G$*Me*$_H$: $\delta k_{ran}/k$ = 0.065, $\delta k/k$ = 0.081; (3) *Me*$_{E\text{-}F}$*Me*$_{G\text{-}H}$: $\delta k_{ran}/k$ = 0.038, $\delta k/k$ = 0.063.

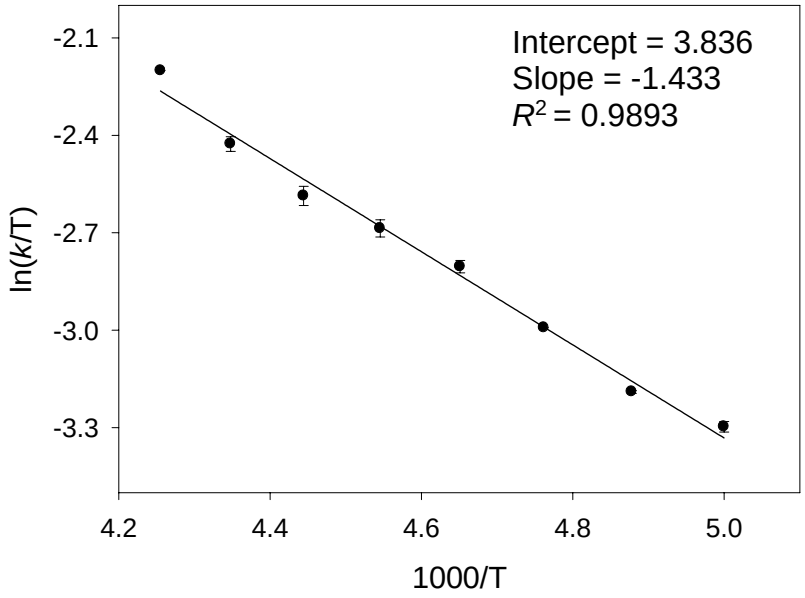


**Fig. S42.** Eyring plot of the $Me_EMe_F$ exchange in Hf-Cl (**2**) yielding activation parameters for the exchange.

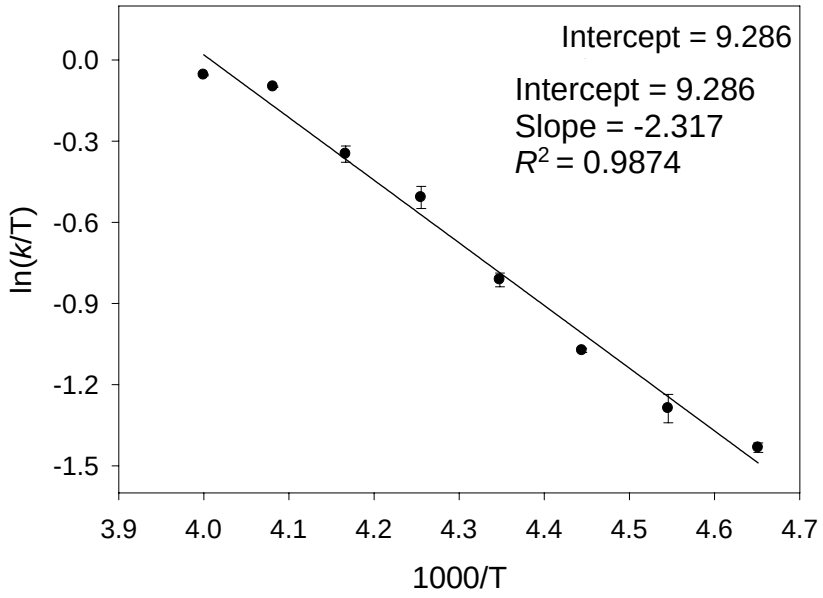


**Fig. S43.** Eyring plot of the $Me_GMe_H$ exchange in Hf-Cl (**2**) yielding activation parameters for the exchange.

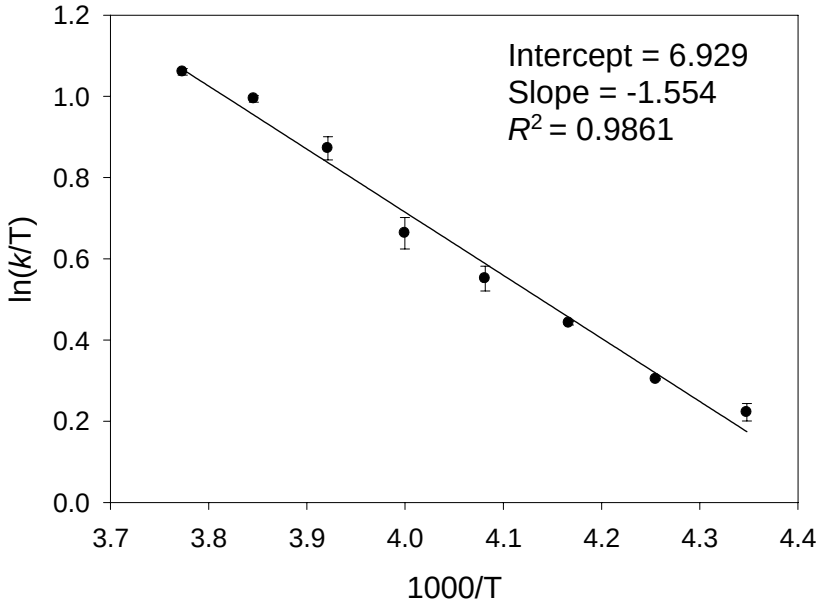


**Fig. S44.** Eyring plot of the $Me_{E\text{-}F}Me_{G\text{-}H}$ exchange in Hf-Cl (**2**) yielding activation parameters for the exchange.

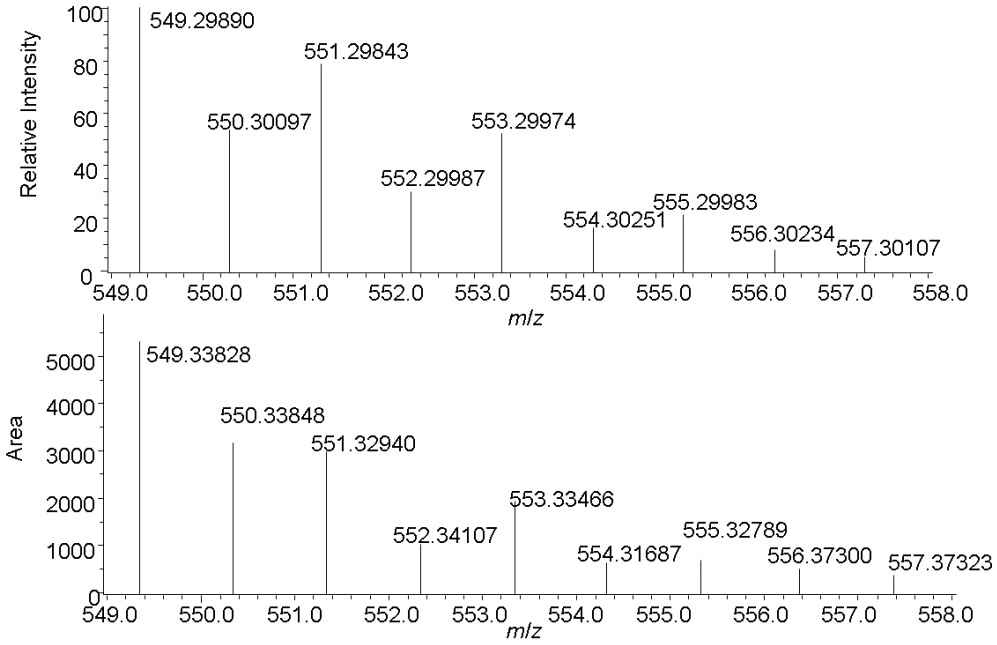


**Fig. S45.** (Top) Calculated and (Bottom) Observed MS for [Zr-Cl (**1**)+H$^+$].

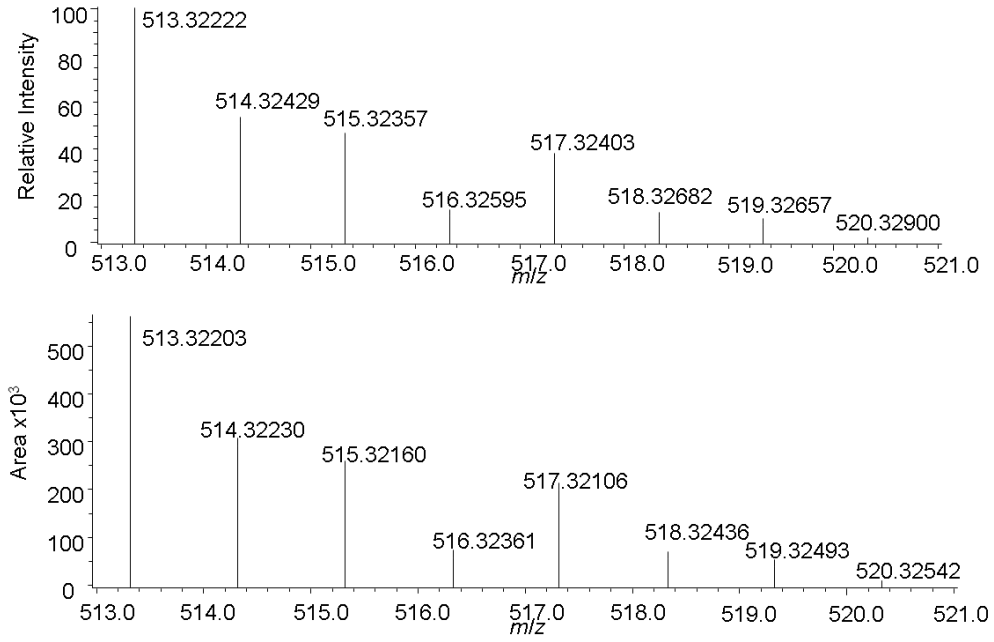


**Fig. S46.** (Top) Calculated and (Bottom) Observed MS for Zr[MeC(N$^i$Pr)$_2$]$_3^+$ (**7**).

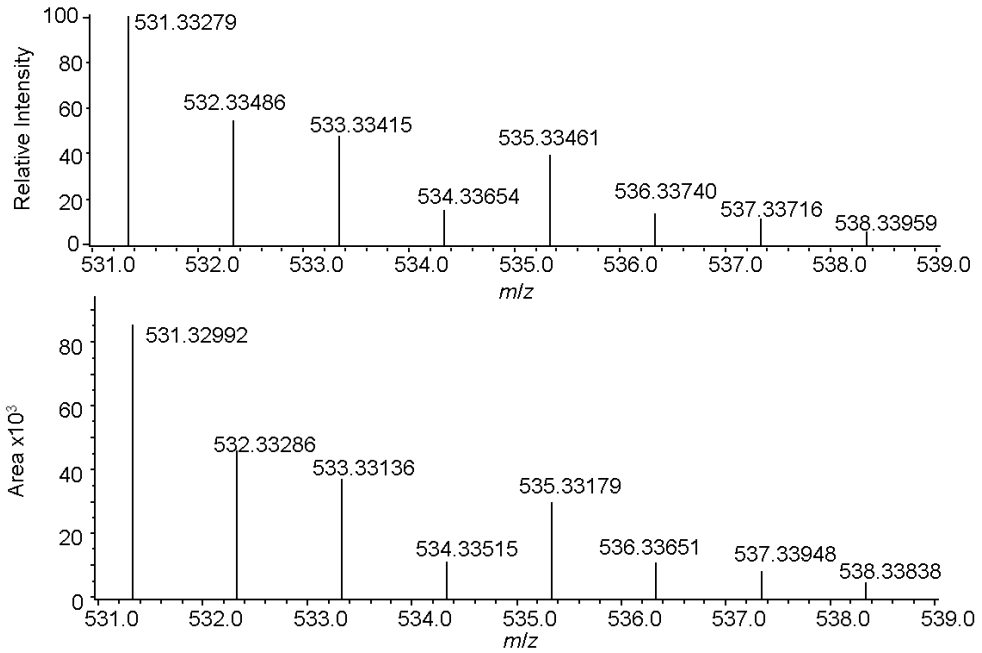


**Fig. S47.** (Top) Calculated and (Bottom) Observed MS of [Zr-OH (**9**)+$H^+$].

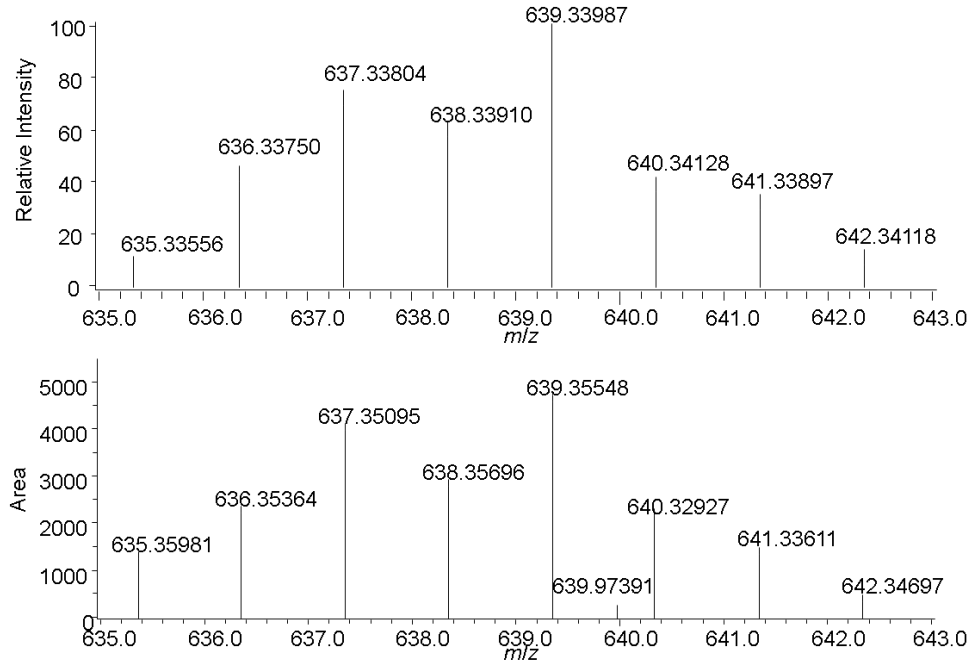


**Fig. S48.** (Top) Calculated and (Bottom) Observed MS for [Hf-Cl (**2**)+$H^+$].

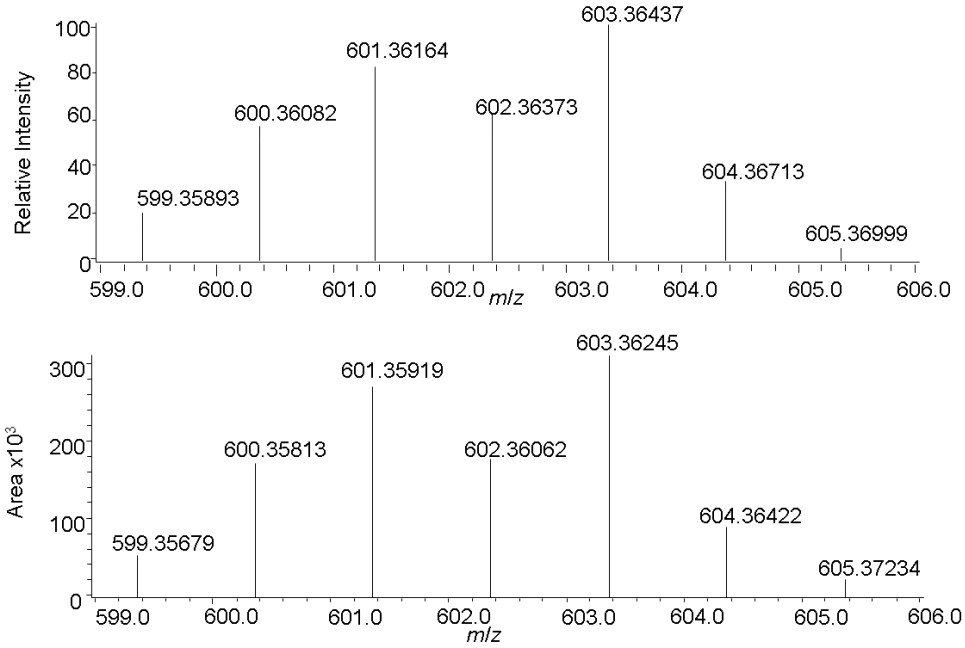


**Fig. S49.** (Top) Calculated and (Bottom) Observed MS for $Hf[MeC(N^iPr)_2]_3^+$ (**8**).

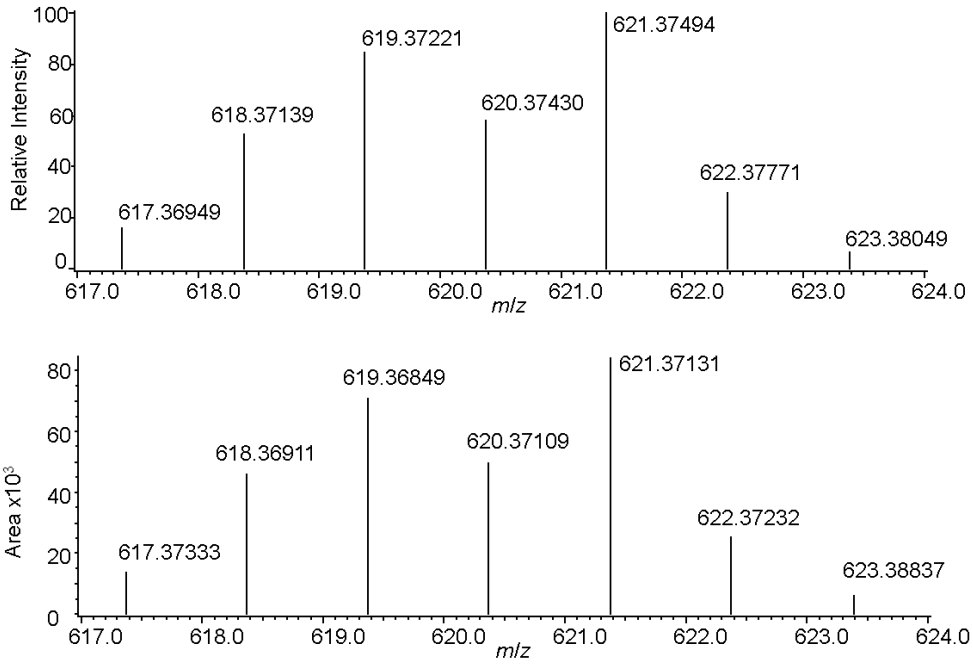


**Fig. S50.** (Top) Calculated and (Bottom) Observed MS of [Hf-OH (**10**)+$H^+$].